Korean J. Chem. Eng., 38(8), 1531-1555 (2021)
DOI: 10.1007/s11814-021-0832-2

pISSN: 0256-1115
eISSN: 1975-7220

REVIEW PAPER

A comprehensive review of membrane fouling and cleaning methods with emphasis on ultrasound-assisted fouling control processes

Masoume Ehsani†, Huu Doan, and Ali Lohi

Department of Chemical Engineering, Ryerson University, 350 Victoria Street, Toronto, ON, M5B 2K3, Canada
(*Received 12 March 2021 • Accepted 29 April 2021*)

Abstract−One of the most critical issues encountered in membrane-based separation processes is permeate flux decline in a system operating for a long period. The particles in the feed solution tend to foul the membrane surface or membrane pores, which results in pore blocking and/or cake formation on the surface. In this regard, the use of membrane cleaning techniques for the membrane flux restoration has gained more attention. Ultrasonic (US) irradiation is an alternative technique applied to the feed solution passing across the membrane surface to either prevent the fouling formation (fouling control) or dislodge the foulants (surface cleaning). Ultrasonic cleaning mechanisms are based on sound waves travelling through the liquid, which leads to physical and chemical effects. This cleaning technique is an environmentally friendly process in which no chemical or biological agents are used. This article briefly reviews different types of fouling and classes of foulants, fouling evolution mechanisms, mathematical modelling of fouling, surface cleaning and fouling control strategies, with the emphasis on ultrasound-assisted fouling control process as an innovative cleaning method. The effect of the operational parameters on the performance of the US-assisted filtration processes, highlights, challenges, and future outlook of US cleaning will be discussed.

Keywords: Fouling Control, Membrane Cleaning, Fouling Modelling, Ultrasound Irradiation

INTRODUCTION

Water scarcity, especially freshwater depletion, is one of the most severe and imminent problems around the world. In this regard, wastewater treatment processes have gained increasing attention to alleviate the water shortage concern. Membrane-based processes are one of the leading technologies applied to industries in response to the wastewater reclamation and clean reusable water production [1].

There is much interest in membrane technology as a separation process because of its high efficiency and very minor harmful impact on the environment [2]. Despite these advantages, membrane fouling is the major drawback in membrane-based processes, which could stop the permeate flow [3]. Membrane fouling occurs due to the solute accumulation and particulate precipitation on the membrane surface along with their deposition within the membrane pores, which consequently increases the membrane resistance and reduces the permeation [4]. Furthermore, fouling formation has an adverse effect on the membrane performance by cutting down the membrane lifetime and increasing the cost of the treatment process due to the frequent physical and chemical cleaning required to remove the foulants [5]. The membrane fouling diversity, as well as its severity, depends on several factors including membrane characteristics, solution properties and operational parameters [6].

Membrane replacement cost is an important factor in a long-term filtration process. Therefore, several processes and technologies have been introduced to control fouling in industrial membrane applications. Membrane cleaning technologies are chosen based on the fouling type and the membrane properties in order to obtain high fouling removal and flux restoration. Pretreatment, chemical cleaning, electrochemical, advanced oxidation, backflushing, pulsing mode, vibration, air sparging and electrical field are some of the commonly used cleaning processes [5,7,8]. Interestingly, during the past two decades the number of studies on membrane fouling and its cleaning process has been remarkably increasing.

The most significant disadvantage, which is responsible for the efficiency decline of the membrane process, is that the abovementioned cleaning methods can rarely be carried out concurrently with the membrane's continual process; thus, the membrane filtration process is required to be stopped for membrane cleaning. Therefore, the ultrasound (US) technique has been recommended and adopted as an innovative approach [7,9]. The US transducers are placed at the membrane module and the US irradiation is performed simultaneously with the filtration process. Ultrasound cleaning is a promising physical method in which foulants are removed and the permeation is improved notably [9,10]. Furthermore, chemical or biological agents are not required in the US application to improve the membrane performance, representing the environmentally friendly aspect of the US-assisted application. Ultrasound mechanism is based on wave propagation generating mechanical power and leading to mechanical movement through the medium because of microbubbles formation (cavitation) at a sufficiently high power [8,11,12].

Micro-jet, micro-streamers, micro-streaming, acoustic streaming, and shock wave effects are also produced during the ultrasonic cavitation, which leads to the particle detachment from the mem-

†To whom correspondence should be addressed.
E-mail: masoume.ehsani@ryerson.ca

brane surface and the decline in the concentration polarization and the cake layer formation. As the US power intensity increases, the collapse of microbubbles occurs violently and releases a substantial amount of energy due to the rapid changes in pressure around microbubbles. Afterwards, the generated energy from ultrasonic cavitation is able to remove the cake layer from the membrane surface and reduce the interaction between foulants and the membrane surface or even the membrane pores [1,8,11,13,14]. Although the application of ultrasound is effective for membrane fouling control, particle aggregation may occur under the ultrasound irradiation without cavitation bubble formation [11].

Ultrasound irradiation is a viable fouling control and cleaning process that has received much attention in recent years. Some researchers have employed the combination of membrane technology and US irradiation for wastewater treatment processes. The effects of operational parameters, such as frequency, power intensity, particle characteristics in feed solutions, membrane properties, and process mode were investigated [1,3,6,15]. The results of those studies indicated that high-efficiency membrane fouling control occurred at low US frequency and high power intensity [7,13, 14,16,17]. Furthermore, distinctive fouling removal efficiency was obtained for ultrafiltration and microfiltration membranes with US transducers installed at different positions [5,10]. However, US irradiation may result in membrane damage in some cases.

The present review article includes an introduction to membrane fouling, effective parameters on foulant deposition, fouling control, and membrane cleaning techniques. Modelling of membrane fouling is also presented so to reach a quantitative determination of membrane fouling determination and elucidate a suitable mechanistic model for the prediction of filtration performance (especially, prediction of permeate flux). The main goal of this review paper is to investigate the influence of ultrasound irradiation on membrane fouling removal, raise the highlights and challenges of using this method, and finally, present the outlook for ultrasound-assisted filtration processes in wastewater treatment industries.

MEMBRANE FOULING

Wastewater streams contain various types of contamination such as microorganisms, organic pollutants, inorganic salts and particles. Membrane-based processes are a promising technology due to their capability for the particulate matter removal [18]. A favorable membrane treatment process leads to a high rejection as well as a high permeate rate. However, the accumulation of solutes on the membrane surface (external fouling) and their deposition in the membrane pores (internal fouling) cause membrane fouling and decay in permeate flux rate. Membrane fouling is a complex physicochemical phenomenon involving the combination of several mechanisms acting synergistically [18]. Fouling characterization and effective parameters on membrane fouling are elaborated as follows.

1. Fouling Characterization

Fouling is an unavoidable phenomenon during the separation process of low molecular-weight or macromolecule contaminants in various types of membrane-based processes. This phenomenon can occur at both the membrane surface and the membrane pores, by sieving and adsorption. The retained particles accumulate on the membrane surface and result in cake formation, which is known as external fouling. The retained contaminants in the mass transfer boundary region cannot diffuse back to the feed solution; therefore, a concentration polarization is formed on the top surface of the membrane, which leads to a reduction in the permeate flux by increasing the transmembrane pressure (TMP). In the sieving mechanism, particles larger than the membrane pore size amass over the pores and make a complete blocking [2,4,6,18-21].

Another primary fouling formation mechanism is adsorption, which is the result of intermolecular interaction between materials. Substances with particle size smaller than the membrane pores enter the pores and are adsorbed to the pore wall, and hence, over time, create pore-blockage. The particle adsorption causes the membrane pore size reduction and the membrane flux decline. This occurs immediately after starting the separation process with a fresh membrane without any solute on its surface. The pore blockage mechanism is considered as an internal fouling, which significantly depends on the particle properties and the membrane material chemistry. The interaction between solutes and the membrane surface involves weak van der Waals forces, electrostatic attraction, and chemical bonding [6,18,22]. The diagrams of sieving, adsorption and cake formation mechanism are depicted in Fig. 1.

External fouling, which occurs due to the deposition of rejected contaminants, is generally considered as reversible fouling. However, both the standard pore blockage and adhesive fouling layer

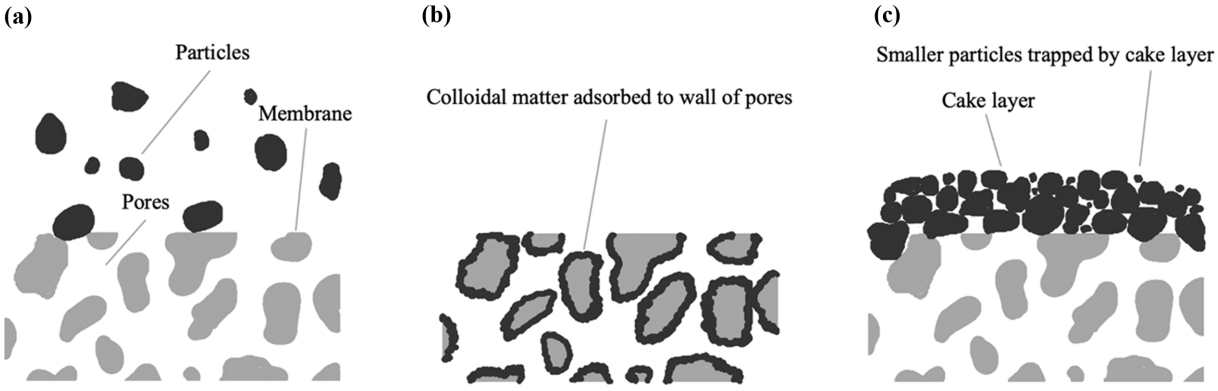

Fig. 1. Schematic diagram of filtration mechanisms and cake formation: (a) sieving, (b) adsorption, (c) cake formation [21].

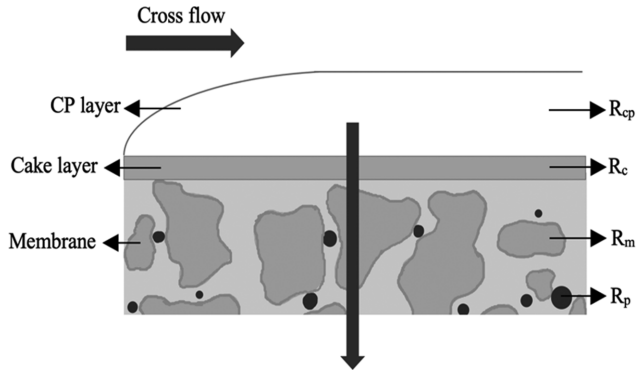

Fig. 2. The major resistances of porous membrane to the permeate stream in a cross-flow filtration [24].

on the top surface of the membrane are irreversible fouling. Reversible and irreversible fouling are distinguished by their resistance towards the cleaning processes. Reversible fouling is easily removed by a physical cleaning process, like membrane washing, while irreversible fouling is more challenging, and it remains on the membrane surface after the physical cleaning process. Irreversible fouling can be removed by chemical cleaning.

The change in the membrane resistance to the permeate stream depends on the type of fouling. The resistance gets larger by standard pore-blocking (R_p); however, it is further increased by cake formation (R_c) due to an additional resistance being incurred to the filtration system [23]. The permeate rate is inversely proportional to the overall membrane resistance. Aside from all fouling formation mechanisms, concentration polarization is another phenomenon that increases the overall resistance over the membrane (R_{cp}). Solute accumulation and high concentration near the boundary of the solid membrane and the effluent render the polarization. This phenomenon causes a higher osmotic pressure, a lower rejection, and a permeate rate decline as well as a potential enhancement of membrane fouling. Concentration polarization is a reversible phenomenon that is easily influenced by the flow velocity [21]. Fig. 2 presents all the major resistances in a porous membrane. R_m describes the inherent membrane resistance.

2. Effective Parameters on Membrane Fouling

2-1. Foulants

The type of contaminant in the feed stream is one of the most important factors playing a prominent role in fouling phenomenon [4]. For instance, in the food industry, organic materials (either soluble or colloidal) such as lipids (fats, oils, and waxes), macromolecules (proteins, carbohydrate, humic acid, and polysaccharides) and antifoam agents represent a challenging problem in membrane filtration processes [4,22]. Macromolecules and fatty acids, which form the oils and fats, are ubiquitous in the waste streams of the food industry. As soon as the feed stream reaches the solid surface, the interaction between the functional groups of the macromolecules and the membrane surface results in cake layer formation [6]. In addition, pore blockage also occurs due to the small size of the fatty acids and their adsorption in membrane pores [25]. Aside from the organic compounds, the presence of soluble mineral salts, such as calcium sulfate, calcium carbonate, calcium phosphate, magnesium salts, silica, metal hydroxides, can also result in fouling formation. Fouling formation was found inevitable in nanofiltration (NF), reverse osmosis (RO), and membrane distillation (MD) applications which are mainly employed for the inorganic solute rejection [4,26].

Reversibility of the fouling layers relies upon the type of solute in aqueous solutions. Li et al. [27] studied the fouling mechanism in a nanofiltration membrane. They used humic acid as a foulant and observed an adhesive force between the fouling layer and the membrane surface, which resulted in an irreversible fouling layer; chemical cleaning was required for fouling mitigation. Mi and Elimelech [28] used sodium alginate (a polysaccharide) as an organic model foulant in a forward osmosis process. The results of their study indicated that the flux recovery was almost 98% after rinsing the fouled membrane with water without application of any chemical reagent. The fouling reversibility of an organic mixture was investigated by Katsoufidou et al. [29] A feed containing humic acids and sodium alginate was used in a UF treatment process. The interaction between the compounds was studied, and the fouling formation of the two individual foulants was compared. The fouling behavior by the mixture was dependent on the foulant proportion. However, the fouling behavior of the mixture was somewhat similar to the sodium alginate scaling, even at a low concentration of this component. Industrial wastewater may contain mixed foulants; accordingly, Choi et al. [30] focused on calcium sulfate ($CaSO_4$) as a common inorganic scalant and silica (SiO_2) as a colloidal particulate in a forward osmosis (FO) system. Their study indicated that the cake layer formation by $CaSO_4$ precipitation was fully reversible. The researchers underscored that the size of the suspended colloids ranges from a few nanometers to few micrometers, and it was almost impossible to separate all colloids smaller than a few hundred nanometers. The result of colloidal fouling was entirely different. The suspended colloids were negatively charged in the neutral pH range and agglomerated on the membrane surface or within the membrane pores due to the presence of opposite charge in the environment. Colloidal fouling was found as irreversible fouling, which required more complicated cleaning processes for the membrane flux recovery.

Membrane fouling also seems to be a critical problem in membrane-based biological processes. Microbial cells and their growth may result in an adhesive fouling layer on membrane surface (biofilm) [18,22,31]. Microbial cells in aqueous solutions produce biopolymers such as extracellular polymeric substances (EPS) and soluble microbial products (SMP). The biopolymeric compounds are composed of proteins, lipids, and polysaccharides which provide a favorable condition for microbial growth and further microbial aggregation [2,4]. Qu et al. [32] investigated the biofilm formation on the UF membrane, by means of the cyanobacterial cells, extracellular organic matter, and their combination. They reported that the cyanobacterial cell aggregation led to both reversible and irreversible fouling. The extracellular organic matter caused adhesive and irreversible fouling layer, and the combination of the biofoulants brought about a remarkable flux decline as a result of more pore blockage and a dense cake layer. Lim and Bai [33] investigated the effect of activated sludge on membrane fouling and flux decline. A microfiltration (MF) module was employed in an acti-

vated sludge bioreactor, and the fouling mechanisms on the MF membrane were studied. Their observation demonstrated that fouling occurred both on the membrane surface and inside the membrane pores. The slough attached cake layer could be removed by water backwashing or sonication while the irreversible biofilm on the surface of the membrane and within the membrane pores was removed by a combination of cleaning processes, including water backwashing, sonication and chemical cleaning. Similar observations were reported by several researchers [19,22,34-36].

2-2. Feed Solution Chemistry

Fouling formation depends on the solution chemistry (pH and ionic strength) due to the different characteristics of the foulant at varied levels of pH and ionic strength. Altering the pH level influences the surface charge of the contaminants as well as their accumulation. The ionic strength, which is directly proportional to the solution conductivity, affects the membrane surface charge, electrical double layer (EDL), and hydrodynamic radius of the foulant. The hydrodynamic radius of the foulant can be reduced and that enables the pore blockage as a result of a high ionic strength [6, 45,46]. Fouling formation intensifies around the isoelectric point (point of zero charge) of the foulants and the membrane since the electrostatic repulsion force between the foulants and the membrane is decreased. The effect of ionic strength and pH on fouling relies upon the type of the foulant and its concentration in solution as well as the chemistry of the membrane surface (hydrophilic or hydrophobic).

Abdelrasoul et al. [47] studied the pH influence on fouling formation of latex solution. A polycarbonate membrane was used in ultrafiltration of a latex paint solution. According to the reported results, ionic strength increased as the pH of the solution was raised from 7 to 14. Fouling attachment also was weakened significantly with increases in the solution pH from 7 to 12 since the zeta potential of particles and the membrane became increasingly negative, which in turn reduced electrostatic attraction both between particle-to-particle and particle-to-membrane. Therefore, increasing the pH value resulted in an enhancement of the membrane hydrophilicity and a significant reduction in particle aggregation, which consequently enhanced the membrane flux and lowered the power consumption. Similar result was reported by Lee et al. [46].

The influence of ionic strength on colloidal fouling in a tubular ceramic membrane was observed by Singh and Song [48]. Silica colloids were used as foulant and NaCl was added to the solution to increase the ionic strength. The results showed a linear relationship between fouling potential and double layer thickness in which the fouling potential enlarged by denser double layer. The fouling potential was tripled as the ionic strength was increased from 0.001 M to 0.1 M. It can be concluded that high ionic strength can result in a denser double layer of counterions and more considerable fouling potential. Singh and Song also worked on the synergistic effect of pH and ionic strength on colloidal fouling [45]. The effect of pH on colloidal silica particles was summarized as follows:

$$\text{-Si-OH}+\text{OH}^- \leftrightarrow \text{-Si-O}^- + \text{H}_2\text{O} \quad (1)$$

$$\text{-Si-O}^- + \text{H}^+ \leftrightarrow \text{-Si-OH} \quad (2)$$

According to reactions 1 and 2, in acidic pH level, the protons were adsorbed by negatively charged silica nanoparticles and formed an intermediate component. Therefore, the electrostatic repulsive force between the particles was reduced and caused cake layer formation. Results of the measured zeta potential also verified the electrostatic repulsive force reduction when the solution pH was decreased. On the other hand, in the alkaline solution the silica nanoparticles were in the negatively charged state by the adsorption of hydroxide ions onto colloidal particles. This helped in increasing the repulsion between particles and reduction in the fouling potential. Additionally, an incremental increase in fouling potential was also observed as the ionic strength increased at all pH levels due to the high ratio of the Na^+ relative to the H^+. At a high ionic strength, the particle attachment decline was smoothed as the pH level was increased, indicating that the increases in the ionic strength had a major impact on fouling potential as compared to the effect of the pH level augmentation.

The effect of monovalent and divalent cations on alginate fouling was studied by Lee et al. [46]. They observed that the alginate fouling was mitigated by increasing the concentration of the divalent cations (Ca^{2+} and Cu^{2+}) due to the formation of larger particles and their back diffusion into the bulk solution. In contrast, adding monovalent cations (in the form of ammonium chloride (NH_4Cl), potassium chloride (KCl), and sodium chloride (NaCl)) into the feed solution resulted in severe fouling formation. In fact, a compact cake layer was created on the membrane surface due to the formation of smaller spherocolloidal macromolecules. Similar results regarding the effect of pH altering and the addition of the monovalent cations on fatty acid fouling of FO membrane were reported by Zhao et al. [49] Lee et al. [50] also studied the influence of pH and ionic strength on the fouling potential of carbon nanotube enhanced filtration membrane. They reported that the performance of the micro-wall carbon nanotube (MWCNT) membrane could be controlled by the feed chemistry. However, the optimal value for pH and ionic strength varied for different types of protein foulants.

2-3. Membrane Properties

Polymeric membranes and inorganic membranes are two types of membrane materials frequently used in industrial applications. The selective membranes are designed to tolerate various operational conditions involving temperature, pressure, and pH altering, and withstand several cleaning processes and cleaning agents as well as having less fouling tendency. Membranes are classified as hydrophilic or hydrophobic. Hydrophilic membranes have a higher permeate flux and are less affected by foulant attraction, which makes them favorable for high-flux separation processes. However, hydrophobic membranes have better physical, thermal and chemical properties [4,51,52].

Membrane properties such as hydrophilicity, surface roughness, and surface charge are among the major factors controlling the fouling behavior at the initial stage of the filtration process. The reported results from various researches point to a definite link between the high surface roughness and the abrupt fouling formation [53-55].

Moreover, if the membrane and the foulant have the same type of surface charge (positive or negative), fouling formation is reduced due to the electrostatic repulsive force. Wang and Tang [56] stud-

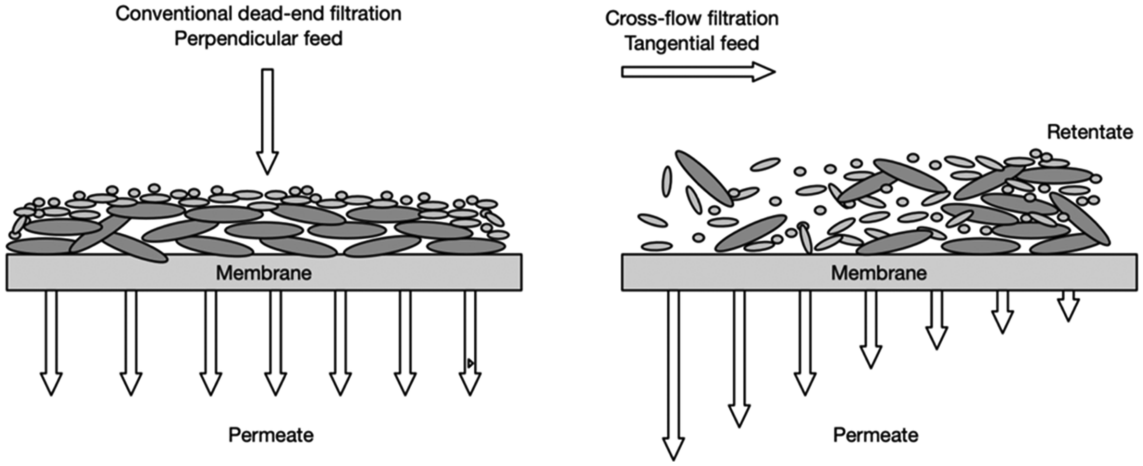

Fig. 3. The fouling formation in dead-end and cross-flow mode filtration [62].

ied the effect of membrane properties on the fouling of negatively charged bovine serum albumin (BSA) molecules over a four day treatment process. They used four types of commercial membranes: one RO, two NF and one UF membranes. Despite all the different properties such as water permeability, salt rejection, hydrophilicity, zeta potential, molecular weight, and surface roughness, in the long run the membranes obtained an almost equal permeate flux. In a long-term process, the fouling formation and flux behavior depended on the foulant-fouled membrane interaction since the membrane surface was fully covered by a cake layer, and additional fouling occurred based on the interaction between foulant and deposited foulant. Whereas, at the initial stage, the fouling was formed due to the foulant-clean membrane interaction, and the permeate flux was influenced by membrane properties. Therefore, membranes with high surface roughness and low hydrophilicity, as well as less negatively charged surface, were more prone to the permeate flux decline at the initial stage.

2-4. Membrane Surface Pore Size

Cake layer formation on the membrane surface or pore blockage can easily reduce the membrane pore cross section or entirely block it. The tight-pores on the membrane surface are indeed plugged gradually or even vanished in a long run of fouling development [57]. However, Nghiem and Hawkes [58] reported that membranes with larger pore size rendered severe fouling. Hwang et al. [59] worked on the influence of membrane pore size on particle fouling. They proposed a blocking index to indicate the level of membrane fouling and reported that a membrane with a larger pore size had a higher blocking index due to the ample space for the particle deposition, which in turn resulted in a faster permeate flux decline. A similar result was obtained by Zeng et al. [60] who studied membrane fouling in filtration of a dextran solution. It was observed that the reversibility of fouling was affected by the intrinsic pore size, and irreversible fouling mostly took place in membranes with larger pores [61].

2-5. Flow Velocity

Membrane filtration is operated under either dead-end or cross-flow mode. In dead-end filtration, the feed stream is pushed through the membrane by pressure. All the feed stream solution entering the filtration system passes through the membrane and there is no rejection flow. The retained solutes may accumulate and create a cake layer having an identical structure over the entire membrane surface. On the other hand, in cross-flow filtration, a tangential feed stream passes over the membrane surface, which reduces the solute accumulation significantly, mostly due to the turbulence flow. In fact, a thin cake layer is observed at the feed entrance turning into a thick layer along the flow path. The comparison of dead-end and cross-flow filtration is presented in Fig. 3.

As depicted in Fig. 3, dead-end filtration is more susceptible to fouling since it lacks the shear stress on the interface in order to detach foulant from the membrane and carried away by the reject stream as in the case of cross-flow filtration. Thus, increase in flow velocity only leads to solute aggregation as well as cake formation compressibility, resulting in a remarkable permeate flux decline [63].

Cross-flow filtration is an excellent mode for the treatment process of aqueous solutions. The fouling probability decline lies in the fact that an increase in the flow velocity causes high shear stress on the membrane surface, leading to foulant detachment and back diffusion that eventually reduces the fouling growth [24,64]. In addition, the residence time of solutes on the membrane surface depends upon the flow velocity. A higher flow rate results in a lower residence time, a lower foulant accumulation probability, and hence, a higher membrane capacity is realized. Thus, it can be concluded that the membrane capacity is directly proportional to the volume of filtered solution [65]. The effect of various cross-flow velocities on membrane performance and fouling behavior was examined by Chen et al. [66]. The finding revealed that fouling formation rate dropped as the cross velocity was increased.

2-6. Process Pressure

During the foulant attachment and deposition on the membrane surface, the concentration of the foulants increases and attains the highest value when maximal foulant packing occurs. At this point, the critical filtration pressure is obtained, which is counterbalanced by the osmotic pressure (maximal value). If the applied pressure is less than the critical pressure, the foulants brought toward the membrane surface could diffuse back to the bulk solution. A further increase in applied pressure beyond the critical pressure

can keep the foulants close to the membrane surface and result in further foulant accumulation and thicker cake layer [67]. Thus, there is a critical point for pressure at which the fouling probability and the permeate flux are expected to level off, i.e., the permeate does not increase further with increases in pressure, and further pressure increase leads to the greater foulant-to-foulant and foulant-to-membrane attachment [13,42,64]. A similar trend was observed by Jain et al. [68] as well. They investigated the synergistic effects of pressure and cross-flow velocity on fouling development. At a lower level of the TMP, pore blockage mainly occurred and, accordingly, cross-flow rate enhancement resulted in a decrease of fouling. For high values of TMP, fouling was predominantly by cake formation, and thus feed flow rate altering could not improve the permeate flux due to the cake layer compressibility.

MODELLING OF FOULING MECHANISMS IN ULTRAFILTRATION (UF) AND MICROFILTRATION (MF) PROCESSES

The flux-time curve for UF and MF process commonly includes three stages. First, a rapid initial flux decline from the flux of pure water filtration is commonly observed. The initial flux decay is followed by a long-term continuous flux decline, and finally, membrane flux reaches a plateau (semi-steady-state condition). The rapid initial flux decline can be elucidated in terms of pore-blocking mechanism since less than one layer of particle deposition is enough to result in significant pore-blockage. However, the severity of the pore-blockage is related to the shape and size of the particles and membrane pores [69]. The experimental results conducted by Jiang et al. [70] also showed that organic solutes and colloidal contaminants were the predominant component of the pore-blocking mechanism, which was completed very quickly in 8 seconds from the start of the filtration process and followed by cake formation until 100 seconds.

Therefore, membrane transport models (mechanistic models) can be beneficial for the prediction of the process performance, estimation of the membrane permeate flux and optimization of the filtration process. Several mechanistic models have been developed in order to provide a better understanding and description of the membrane fouling formation and the permeate flux decay with filtration time. Mechanistic models are thus needed for the prediction of the fouling mechanism (pore-blocking or cake formation) and control of the fouling development during the filtration process [71,72]. This section starts with an overview of the general filtration equation, the intrinsic resistance of the clean membrane, and the resistance caused by each of the fouling mechanisms. The fouling resistance can be calculated from the permeate flux during the pore-blockage and cake formation. Therefore, models for the estimation of the permeate flux during the pore blockage and cake formation are reviewed.

According to the Darcy law and resistance-in-series model, the general filtration equation is expresses as follows [73]:

$$J = \frac{1}{A_m}\frac{dV}{dt} = \frac{\Delta P}{\mu R_{tot}} = \frac{\Delta P}{\mu(R_m + R_p + R_c)} \quad (1)$$

where J is the permeate flux, A_m the total membrane surface, V the cumulative permeate volume at a given time (t), ΔP the applied pressure, μ the dynamic viscosity, R_m, R_p, and R_c are the resistances of the clean membrane, pore-blockage, and cake layer, respectively.

The equation for the permeate flux can also be rewritten by considering the reversible and irreversible fouling resistances in filtration process [74]:

$$J = \frac{\Delta P}{\mu(R_m + R_r + R_{ir})} \quad (2)$$

where R_r and R_{ir} represent the reversible and irreversible fouling resistances, respectively.

As mentioned, reversible fouling can be removed easily by membrane washing. Thus, the resistance of the irreversible fouling can be determined as below:

$$R_{ir} = \frac{\Delta P}{\mu J'} - R_m \quad (3)$$

where J′ is the permeate flux after the membrane washing.

The very first step in determining the fouling resistance and permeate flux decay due to each fouling mechanism is the determination of the resistance of the clean membrane. Therefore, it is needed to have the water flux through a clean membrane with pure water used as a feed.

It is assumed that all the membrane pores are identical cylinders, and the flow inside the membrane pores is a fully-developed and a steady-state laminar flow. Thus, the flow rate (Q_P) through a single, clean pore can be determined by Hagen-Poiseuille's equation [75]:

$$Q_P = \frac{\pi \Delta P_m D_{P,m}^4}{128 \mu \delta_m} \quad (4)$$

where ΔP_m is the pressure differential through membrane, $\Delta_{P,m}$ pore diameter, and δ_m the membrane thickness.

The velocity inside the membrane pores (v_P) is calculated as follows [75]:

$$v_P = \frac{Q_P}{A_P} = \frac{4Q_P}{\pi D_{P,m}^2} \quad (5)$$

The number of pores per unit area of membrane and membrane porosity (ε) are defined by the following [75]:

$$N_P = \frac{J}{Q_P} \quad (6)$$

And

$$\varepsilon = \frac{A_{P,tot}}{A_m} = N_P A_P \quad (7)$$

where A_p and $A_{p,tot}$ are the cross-sectional area of a single pore and the total area of all membrane pores, respectively.

Therefore, the clean membrane flux and clean membrane resistance can be expressed as follows [75]:

$$J = \frac{\Delta P_m}{\mu R_m} = Q_P N_P = \frac{\pi \Delta P_m D_{P,m}^4}{128 \mu \delta_m} N_P \quad (8)$$

And:

$$R_m = \frac{128\delta_m}{\pi D_{P,m}^4 N_P} = \frac{32\delta_m}{\varepsilon D_{P,m}^2} \quad (9)$$

Eq. (9) indicates that the resistance of the clean membrane is a function of the physical property of the membrane.

The limitation of this model is that removal of the reversible fouling portion may be fluctuating between different runs/experiments since the structure of the fouling (reversible and irreversible) may vary among the runs. Therefore, the value for the measured reversible, and hence, calculated irreversible can vary among the runs, leading to a large standard deviation of the value. Moreover, in reality, the pores of membranes are not perfectly straight cylinder. That is why the concept of tortuosity was introduced to take care of non-straight pores. The assumption of straight cylindrical pores would lead to a significant deviation between the model prediction and actual values.

The development of a more accurate mathematical model of membrane fouling requires the consideration of more details of the types of fouling that may occur during the filtration. Pore-blockage is the first mechanism taking place when the filtration process commences. Pore-blocking includes three different types: complete pore-blocking, internal pore-blocking, and partial pore-blocking [72]. Complete blocking occurs as the foulants completely block the pores, which in turn decreases the active filtering surface area. For the internal pore-blocking, it was assumed that very small particles, compared to the pore radius, deposited on the pore wall as a monolayer and reduced the pore radius. Internal clogging and monolayer formation on the pore wall cannot significantly affect the flux decline, and hence, it may not be considered as one of the main fouling contributors. Therefore, the pressure drop across this monolayer can be neglected. Also, the pore length does not change over the monolayer formation [75,76]. During the filtration process, foulants can partially block the membrane pores (partial clogging). In this case, the size of the foulant is smaller than the membrane pore diameter, and pore-blocking occurs by the accumulation of the foulants inside the membrane pores [76].

Foulant deposition on the membrane surface and cake layer formation can occur concurrently with the pore blockage and cause filtrate flux decay. Cake layer property and flux decline trend can vary in different filtration modes. In the infinite cross-flow filtration, the fouling formation proceeds endlessly until the permeate flux vanishes. On the contrary, in the finite cross-flow filtration, a thin cake layer is observed at the feed entrance, which turns into a thick layer along the flow path. In this case, a cake layer is formed and grown over time until it reaches a constant thickness, which is known as the equilibrium thickness. Accordingly, the permeate flux decreases continuously until it reaches a plateau (steady-state regime) [69].

Field et al. [77] proposed the critical flux theory describing the maximal permeate flux before the fouling development, and estimating the membrane flux during the pore-blocking or cake formation in a cross-flow MF membrane. They modified Hermia's model, which was recommended for the pore-blocking and cake formation in a dead-end filtration (constant pressure), by adding a convective removal term applicable to a cross-flow UF process. The mathematical model suggested by Hermia is expressed as [78]:

$$\frac{d^2t}{dV^2} = K\left(\frac{dt}{dV}\right)^n \quad (10)$$

where V is the cumulative permeate volume at time t, k and n are constants that can be varied dependent on the fouling mechanisms.

Hermia's model was modified and used for cross-flow filtration by adding a convective removal term [77]:

$$-\frac{dJ}{dt}(J^{m-2}) = K(J - J^*) \quad (11)$$

In this equation, J^* is defined as the critical flux (convective term). As long as the permeate flux is equal or less than the critical flux, permeate flux decline is not observed with time. Therefore, the permeate flux equations for different fouling mechanisms were proposed as follows:

$$\text{m=2; complete pore-blocking, } J = J_c + (J_0 - J_c)e^{\left(-\left(\frac{J_0\sigma}{\varepsilon_0}\right)t\right)} \quad (12)$$
$$J_c = B\varepsilon_0/\sigma$$

$$\text{m=1.5; internal pore-blocking, } \frac{1}{J^{1/2}} = \frac{1}{J_0^{1/2}} + \left(\frac{K_s'}{2}\right)A^{1/2}t \quad (13)$$

$$\text{m=1; partial pore-blocking, } \sigma t = \frac{1}{J_i}\ln\left(\frac{J}{J_0}\frac{(J_0 - J_i)}{(J - J_i)}\right) \quad (14)$$
$$J_i = B'/\sigma$$

$$\text{m=0; Cake formation, } \frac{\alpha k_c}{J_0 R_m}t = \frac{1}{J_s^2}\left[\ln\left(\frac{J}{J_0}\frac{(J_0 - J_s)}{(J - J_s)}\right) - J_s\left(\frac{1}{J} - \frac{1}{J_0}\right)\right] \quad (15)$$
$$J_s = S/k_c$$

where J_0 is the initial permeate flux, J_c, J_i, and J_s are the critical fluxes at different m values, ε_0 the clean membrane porosity, σ the area of blocked membrane per unit volume of the permeate, K_s' Hermia's parameter for internal pore-blocking, B a constant, B′ a back flux factor, A the membrane surface, S the rate of cake erosion, α the specific resistance of cake, and k_c the cake filtration constant.

Fouling development and thickness of the cake layer is not identical over different regions of the membrane, and inhomogeneity of the foulant deposition over the membrane surface is needed to be considered in estimating the steady-state flux. Pore clogging can occur at a different time during the filtration process. Afterwards, particle deposition and cake formation take place on the blocked portion of the membrane surface. Therefore, the cake layer at different regions of the membrane may have different thickness and age. Besides inhomogeneous cake formation, the flux decay over the internal and partial blocking are neglected in some studies, and complete blocking is the only mechanism considered for modelling of the filtration process and estimation of the membrane permeate flux. According to the mechanistic model proposed by Lianfa Song [69], the number of membrane pores blocked by foulants is directly proportional to the bulk suspension volume. Hence, the pore-blocking rate can be described as follows:

$$\frac{dn}{dt} = -f_{block}\frac{J_0}{n_0}c_0 n = -\alpha n \quad (16)$$

$$\alpha = \left(-f_{block}\frac{J_0 c_0}{n_0}\right) = \text{blocking coefficient} \quad (17)$$
$$n = n_0 e^{-\alpha t}$$

where J_0c_0 represents the particle deposition rate on the clean membrane, n the available membrane pores at any time, n_0 the initial number of available membrane pores, and f_{block} the number of pores blocking by a unit volume of foulants. According to this equation, the fraction of unblocked and blocked surface is $e^{-\alpha t}$ and $(1-e^{-\alpha t})$, respectively. Thus, the time-dependent permeate flux during the pore-blockage can be determined as follows [69]:

$$J=J_0e^{-\alpha t}+J_{p0}\,(1-e^{-\alpha t}) \tag{18}$$

where J_0 is the initial permeate flux and J_{p0} the flux of the blocked membrane. The ultimate permeate flux in this study verifies the model, developed by Field et al. [77], for estimation of the permeate flux during the complete pore blocking.

For estimation of the permeate flux during the cake formation, the author developed the time-dependent cake formation models to precisely describe the flux decay in an infinite cross-flow filtration process (similar to the dead-end process). It was assumed that the cake layer was created right after the complete pore-clogging. The ultimate permeate flux after the membrane fouling in an infinite cross-flow filtration was expressed as follows [69]:

$$J_{(t)}=e^{-\alpha t}\frac{\Delta P}{\mu(R_m)}+(1-e^{-\alpha t})\frac{\Delta P}{\mu(R_m+R_p)}\times\left(1+\frac{2r_c(\Delta P)}{\mu(R_m+R_p)^2}\frac{c_0}{c_g}t\right)^{-1/2} \tag{19}$$

where c_0 is the particle concentration in the bulk suspension, c_g the particle concentration at membrane surface, and r_c the specific resistance of cake layer. As can be seen in Eq. (19), the permeate flux becomes zero at the end of the process, i.e., at an infinite length or a time t approaching infinity, which is similar to the dead-end filtration.

Another mechanistic model on the combination of the pore blockage and cake formation in a stirred ultrafiltration cell (dead-end filtration) was developed by Ho and Zydney [79]. The model was developed with an assumption of an inhomogeneous cake layer formation over different regions of the membrane surface. After a certain period, large proteins aggregated and deposited on the membrane surface and reduced the available filtration area. Additionally, the protein deposition and fouling layer formation resulted in an increase in hydraulic resistance, which reduced the permeate flux. However, it was assumed that the blocked pores and fouled membrane were partially permeable and there was a small finite flow through the membrane pores. Hence, the volumetric filtrate flow rate for open and blocked pores was determined as below:

$$Q_{open}=\frac{\Delta P}{\mu R_m}A_{open}\ \text{in which}\ J_{open}=\frac{\Delta P}{\mu R_m} \tag{20}$$

$$Q_{blocked}=\int_{A_{blocked}}\frac{\Delta P}{\mu(R_m+R_{pp})}dA_{blocked}\ \text{in which}\ J_{blocked}=\frac{\Delta P}{\mu(R_m+R_{pp})} \tag{21}$$

where R_{pp} is the resistance of protein deposit and it was expressed as follows:

$$R_{pp}=(R_m+R_{pp0})\sqrt{1+\frac{2f'R'\Delta PC_b}{\mu(R_m+R_{pp0})^2}(t-t_P)}-R_m \tag{22}$$

where f′ is the fraction of proteins contributing to the growth of the deposit, R′ the specific resistance of protein layer, C_b the bulk protein concentration, the t_P time at which the initial deposition occurs and R_{pp0} the resistance of a single protein aggregate, and can be estimated by using the Kozeny-Carman equation.

$$R_{pp0}=\frac{5\delta_m}{\varepsilon S^2} \tag{23}$$

where δ_m, ε, and S are the thickness, porosity and specific surface area of the deposited proteins layer, respectively. According to this equation, the maximal value for R_{pp} at any time (t) will be achieved with t_P=0.

The approximate ultimate flow rate of the fouled membrane over the filtration time was determined by the following equation:

$$Q=Q_0\left[\exp\left(-\frac{\alpha\Delta PC_b}{\mu R_m}t\right)+\frac{R_m}{R_m+R_{pp}}\left(1-\exp\left(-\frac{\alpha\Delta PC_b}{\mu R_m}t\right)\right)\right] \tag{24}$$

where α is the pore blockage parameter. It was assumed that the deposited protein layer has a uniform resistance. As shown in Eq. (24), the maximum value of the volumetric flux, which is equal to Q_0, can be obtained when t=0. The final volumetric flux involves two terms of flow rate through the blocked pores and protein deposition layer (cake layer). As long as $t_P \gg \frac{\alpha\Delta PC_b}{\mu R_m}$, the volumetric flux is dominated by second term (classical cake filtration model) and proportional to the ratio of the clean membrane resistance over the total resistance.

In all aforementioned studies, the ultimate membrane flux after occurrence of each particular fouling mechanism or combination of complete blocking and cake formation was described. However, during the filtration process, any other combination of the fouling mechanisms can occur. In this regard, the combined fouling models (internal blocking-cake formation, partial blocking-cake formation, complete blocking-cake formation, internal blocking-partial blocking, and partial blocking-complete blocking) were proposed by Bolton et al. [80] for the estimation of the cumulative filtrate volume. All the fouling models were developed for a constant pressure filtration process. A summary of the proposed models is given below:

Complete blocking-cake formation:

$$V=\frac{J_0}{K_b}\left(1-\exp\left(\frac{-K_b}{K_cJ_0^2}(\sqrt{1+2K_cJ_0^2t}-1)\right)\right) \tag{25}$$

Partial blocking-cake formation:

$$V=\frac{1}{K_i}\ln\left(1+\frac{K_i}{K_cJ_0}((1+2K_cJ_0^2t)^{1/2}-1)\right) \tag{26}$$

Partial blocking-complete blocking:

$$V=\frac{J_0}{K_b}\left(1-\exp\left(\frac{2K_bt}{2+K_sJ_0t}\right)\right) \tag{27}$$

Internal blocking-partial blocking:

$$V=\frac{1}{K_i}\ln\left(1+\frac{2K_iJ_0t}{2+K_sJ_0t}\right) \tag{28}$$

Internal blocking-cake formation

$$V=\frac{2}{K_s}\left(\beta\cos\left(\frac{2\pi}{3}-\frac{1}{3}\arccos(\alpha)\right)+\frac{1}{3}\right) \tag{29}$$

$$\alpha=\frac{8}{27\beta^3}+\frac{4K_s}{3\beta^3K_cJ_0}-\frac{4K_s^2t}{3\beta^3K_c},\ \beta=\sqrt{\frac{4}{9}+\frac{4K_s}{3K_cJ_0}+\frac{2K_s^2t}{3K_c}} \tag{30}$$

where K_b is the complete blocking constant, K_c the cake formation constant, K_i the partial blocking constant, and K_s the internal blocking constant.

The above models were validated against the experimental data collected from the filtration of the bovine serum albumin (BSA) and human plasma IgG solutions. It was reported that the complete blocking-cake formation model provided the most accurate fit to the data. However, partial blocking-cake formation and internal blocking-cake formation models also proved to be a good fit to the experimental data. It was also noted that the proposed theoretical models are numerically simple and can be used to estimate the cumulative permeate volume as a function of time. However, the models seemed to be less useful for the determination of the physical parameters, as compared with the model proposed by Ho and Zydney [79].

Mondal and De [81] also proposed a combined model (sequential partial blocking-cake formation) according to Hermia's model [78] and the modified equation developed by Field et al. [77]. The common drawback in all proposed models is that the simultaneous effect of different fouling mechanisms is not considered in those studies. In all those combined models, it was assumed that the pore blocking had occurred at the beginning of the filtration process, and it was followed by the foulant deposition on the membrane surface. Unlike the previous studies, in the model generated by Nguyen et al. [82], it was assumed that cake formation and pore-blockage occurred simultaneously, and the combined model was modified accordingly to this condition. The proposed model was employed for the estimation of the permeate flux during a cross-flow filtration. The pore blockage and the compressive cake layer model were considered in formulating the ultimate filtrate model. The model developed by Ho and Zydney [75] was employed in their study to estimate the permeate flux over the blocked membrane. Therefore, the permeate flux over clean membrane and the rate of the pore-blockage are expressed as follows:

$$Q_{open}=\frac{P_{mf}}{\mu R_m}A_{open} \tag{31}$$

$$\frac{dA_{open}}{dt}=-\alpha Q_{open}C_m=-\alpha Q_{open}\rho\phi_m \tag{32}$$

$$q_{open}=\frac{A_{open}}{A_0}=\exp\left(\int_0^t \alpha\rho\frac{P_{mf}}{\mu R_m}\phi_m dt\right) \tag{33}$$

where P_{mf}, C_m, ϕ_m, and α are the fluid pressure at the membrane surface, protein concentration in the vicinity of the membrane surface, the volume fraction of the solid particles, and the pore blockage parameter, respectively.

The permeate flux though the open pores and the blocked area are described by the following equations:

$$J_{open}=\frac{P_{mf}}{\mu R_m}a_{open} \tag{34}$$

and

$$J_{blocked}=\frac{P_{mf}}{\mu(R_m+R_{pp0})}(1-a_{open}) \tag{35}$$

where R_{pp0} is the initial resistance of the deposit. Indeed, f′R′ (the rate of increase of the blocked region) was omitted in this study since all fouling mechanisms were considered to grow simultaneously and there was no subsequent deposition growth over the blocked region. Thus, the resistance of the blocked area remained constant (R_m+R_{pp0}).

Therefore, the ultimate permeate flux is expressed as follows:

$$J=\frac{P_{mf}}{\mu R_m}\left[\exp\left(\int_0^t \alpha\rho\frac{P_{mf}}{\mu R_m}\phi_m dt\right)+\frac{R_m}{R_m+R_{pp0}}\left(1-\exp\left(-\int_0^t \alpha\rho\frac{P_{mf}}{\mu R_m}\phi_m dt\right)\right)\right] \tag{36}$$

In this modified equation, P_{mf} is not equal to ΔP owing to the presence of cake layer on the membrane surface and it varies over time. Thus, the pressure distribution in the cake layer is needed to estimate the ultimate filtrate flux. The compressive yield stress model proposed by Landman et al. [83] can be employed to determine the pressure distribution in compressive cake layer.

As it is evident, most of the previous studies on the modelling of fouling phenomena were based on a constant-pressure process, and authors developed and used the fouling models for the estimation of the permeate flux, the flow rate, or the cumulative permeate volume. A few studies were on the development of fouling models for constant-flux processes; hence, the developed models were used to estimate the TMP during the filtration process. Kirschner et al. [84] worked on fouling formation mechanisms in a constant flux mode of a cross-flow ultrafiltration process. Their finding indicated that the combined model of partial blocking-cake formation provided the best fit to the experimental data obtained in a constant-flux mode. The complete pore-blocking model, generated based on Hermia's model, yielded a good agreement with experimental data of a constant-pressure process, and a constant-pressure could be applied to the system even with no open pores. However, considering the complete blocking model, a system running under a constant flux is not feasible since there are no open pores for water transport. Similar to the complete blocking mechanism, the pore radius may be reduced or even totally blocked during the internal blocking, which results in zero permeate flux. Estimations of the TMP as a function of filtration time of a constant flux process, under different fouling mechanisms, can be done using the following equations:

Complete blocking:

$$\Delta P_t=\frac{\Delta P_0}{\left(1-\frac{\sigma J}{G}(1-\exp(-Gt))\right)} \tag{37}$$

Partial blocking:

$$\Delta P_t=\frac{\Delta P_0}{\left(\frac{1}{K_i}+\left(1-\frac{1}{K_i}\right)\exp(-K_iGt)\right)} \tag{38}$$

Cake formation:

$$\Delta P_t=\Delta P_0(1+K_cJt) \tag{39}$$

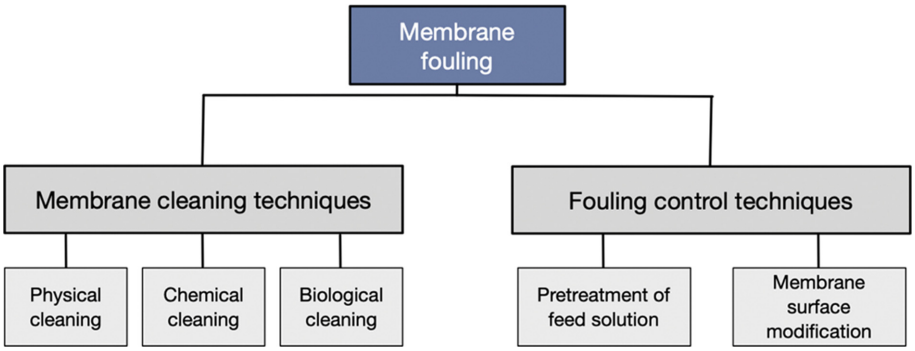

Fig. 4. Different approaches for membrane fouling mitigation.

Internal blocking:

$$\Delta P_t = \frac{\Delta P_0}{(1 - K_s a_0 J t)^2} \quad (40)$$

Combined partial blocking-cake formation model:

$$\Delta P_t = \frac{\Delta P_0 (1 + K_c J t)}{\left(\frac{1}{K_i} + \left(1 - \frac{1}{K_i}\right)\exp(-K_i G t)\right)} \quad (41)$$

where ΔP_t is the TMP at time t, ΔP_0 the initial TMP, J is the constant flux, σ the blocked surface area per unit filtrate volume, G the resuspension factor, K_i the partial blocking constant, K_c the cake formation constant, K_s the internal blocking constant, and a_0 the initial clean membrane surface area.

As mentioned, mechanistic mathematical models can be helpful for the prediction of effective parameters on fouling development or permeate flux, and provide a comprehensive understanding of the fouling phenomenon in practical applications. Using the mathematical models could provide information and details about the type of fouling or any combination of fouling formation that occurs in each particular filtration process. However, it is important to note that a mechanistic model is dependent on all the physical and chemical factors related to the operational parameters, and thus it needs to be modified accordingly for each specific system. In all the aforementioned studies, mechanistic models were generated only for the fouling development in filtration processes. If the membrane cleaning or control processes are employed in membrane filtration, the mechanisms of fouling development need to be investigated so to obtain a model in which all the parameters related to the filtration and cleaning processes are incorporated.

FOULING CONTROL AND MEMBRANE CLEANING

Although different materials have specific and distinctive fouling propensity, this complex phenomenon cannot be totally avoided even with fouling-resistance membranes. Therefore, the subsequent cleaning process is always required to control this adverse phenomenon and improve the filtration rate [85]. The cleaning process is recommended to apply in a correct time after the fouling development since it is more arduous to relieve of the aged foulant [86]. Aside from membrane cleaning, all applicable approaches should be evaluated to achieve an effective method for membrane fouling mitigation. Different approaches for membrane cleaning and fouling control, depicted in Fig. 4, will be discussed in the following subsections.

1. Pretreatment of Feed Solutions

This method is widely exploited at the initial step to avoid a rapid membrane fouling by removing the solute and preventing its deposition on the membrane surface or within the membrane pores. This process generally can be done by either physical or chemical techniques. In the physical technique, a pre-filter or adsorbent is commonly used to remove foulants, which are discarded due to their fouling propensity. For the chemical pre-treatment, anti-scalants or disinfectants are added to the solution to facilitate precipitation, coagulation, or flocculation of the particulates in the feed [18]. A proper pre-treatment method should be adopted with regard to the solution quality and fouling propensity of the solutes. Yang et al. [87] employed different polymeric membranes (UF, NF, RO) as a pre-filter for the inorganic salt removal and fouling mitigation in a pressure retarded osmosis (PRO) power co-generation process. The reported results indicated that only NF and RO processes were effective for scalant removal. The generated power density by the PRO co-generation process with the prefiltration using the NF and RO membranes was 89.3% and 93% of the initial power density, respectively, after a 6-h test (initial power densities were 8.17 W/m^2 and 9.03 W/m^2). However, this value was only 40% of the initial power density of 7.3 W/m^2 for the PRO process without any pre-treatment.

As a chemical pre-treatment, the coagulation pre-treatment of inorganic salts in the feed stream was carried out by Wan et al. [88] Aluminum chloride ($AlCl_3$) and sodium aluminate ($NaAlO_2$) were used for phosphate removal. The untreated solution resulted in more than 50% reduction in the permeate flux, as compared with the initial flux. For the case with the feed pre-treatment, this value was attenuated to be about 30% of the initial flux. Moreover, the initial flux was also increased by more than 13% with the feed pre-treatment. Javeed et al. [89] investigated the effectiveness of iron (III) chloride ($FeCl_3$) and powdered activated carbon (PAC) for flocculation and adsorption of the feed, respectively. As expected, the modified fouling index (MFI) dropped off, notably by increasing the $FeCl_3$ dosage. The results revealed a similar trend with increases in the PAC dosage, although the MFI values remained constant at initial steps with lower amount of PAC. The combination of different pre-treatment methods and its effect on the organic fouling of a RO membrane was proposed by Zhang et al.

[90]. The pretreatment process was a combination of advanced oxidation (ozonation), prefiltration with a ceramic MF membrane, and biological activated carbon (BAC). It was found that the combined pretreatment improved the RO efficiency significantly and a simple deionized water washing dislodged the foulants from the membrane surface.

2. Physical Cleaning Method

Physical cleaning is a common strategy for detachment of substances that are not an integral part of the membrane. This method generally takes place by applying hydraulic, mechanical or electrical forces to dislodge the deposited solutes. Applying the hydraulic and mechanical forces such as reversing TMP (backwashing), turbulence enhancement (rotating disk), or mechanical scouring (air, sponge ball) results in shear stress creation on the membrane surface. In physical cleaning using electrical forces, a voltage is applied along the membrane, which eventually leads to the charged foulant removal [6]. In the following section, common physical cleaning methods will be discussed.

Hydraulic washing/flushing/rinsing reduces the membrane fouling utilizing a turbulent cross-flow over the membrane surface. In practice, the washing flow is carried out in low fouled systems or as an after-treatment process to remove the remaining foulants from other cleaning processes [6].

Backwashing, also known as backflushing or back-pulsing, is frequently used in cross-flow filtration processes for foulant removal and flux recovery. In this method, the filtrate/permeate is pumped backward through the membrane into the feed side in order to provide a periodic backwash. This backward flow dislodges the deposited particles and improves the membrane permeability. The applied pressure in backwashing is higher than the operating filtration pressure. The faster rate of the backwashing, known as back-pulsing, was reported to be more effective [18]. The backwashing flux, duration and frequency are the important parameters in this technique, which can be varied for different types of membranes [22]. Abdelrasoul et al. [91] worked on the effectiveness of the liquid and gas backwashing for flux recovery of a UF membrane, which was used to filter a latex paint effluent. It was reported that the cross-flow water backwashing could recover up to 60% of the permeate flux in a polycarbonate flat sheet membrane whilst the flux restoration was almost 28% with the gas backwashing. The created shear stress by the air washing was not sufficient for the pore-blocking foulant detachment. However, the combination of water and gas backwashing yielded a substantial flux recovery of 75%. Membrane damage can occur under the backwashing process; thus, this method is usually applied to the capillary and ceramic membranes which can tolerate a high reversed rinsing flow [6]. Sondhi and Bhave [92] studied the role of high pressure back-pulsing in fouling mitigation of a cross-flow ceramic membrane. They reported 100% flux recovery by utilizing back-pulsing. This method is also employed in several industrial applications including yeast filtration, slurry filtration, and oily wastewater filtration. The results obtained in those industries showed a long-term fouling reduction as well as a high product recovery.

Turbulence or vortices promotions are among the numerous methods using fluid hydrodynamic altering and shear stress production for fouling reduction. In this process, the inserts, which act as turbulence promoters, installed in the system cause a mixing flow perpendicular to the membrane surface. This phenomenon leads to a high shear rate on the membrane surface and results in the particle back-transport to the bulk solution. Particles are indeed less likely to deposit on the membrane surface or within the pores in turbulence flow. Despite the high energy consumption of cross-flow velocity altering, the inserts are economically viable tools for turbulence flow production and increasing the wall shear rate. The inserts are in several shapes and sizes such as static rods, metal grills, cone shape, spiral wire, disk shape, twisted tapes, Kenics mixer, and a doughnut shape [18,93]. Krstić et al. [94] employed the Kenics static mixer for flux improvement in cross-flow microfiltration of skim milk. Flux improvement of more than 500% was observed at the same Reynolds numbers in the range 3,000-10,000. It was also indicated that lower power consumption was possible, using the inserts to achieve the required turbulence flow for foulant detachment, as compared with the filtration without the promoters. In experiments at the same hydraulic dissipated power, flux improvement of more than 300% was obtained by using the Kenics static mixer. Jokic et al. [95] studied the same topic and used yeast suspension as the feed solution. Flux improvement of 89%-259% was achieved, depending on different design variable values.

Air scouring and gas sparging have been widely exploited in recent years for membrane cleaning and flux restoration. In this method, the air or other gases are directly injected into the concentrate compartment, which creates a two-phase flow, resulting in the shear rate enhancement across the membrane [16]. Flux enhancement in microfiltration of the whey solution by the gas sparging method was studied by Fouladitajar et al. [96]. At the initial stage with a low gas velocity, it was reported that the gas sparging did not seem to be effective in improving the membrane permeability since the injected gas generated a sparsely bubbly flow. However, at a higher gas flow, a turbulence stream was created, leading to the membrane flux recovery and the permeate flux augmentation. Despite the fact that air sparging is considered as a very effective method for fouling reduction of hollow fibre membranes, it is not a practical method such as applying the vortex promoters [23].

3. Chemical Cleaning Method

Chemical cleaning is generally employed for irreversible fouling remediation by using chemical agents including acids, alkalis, oxidants, and surfactants. A mixture of all those materials is commonly used in commercial chemical cleaning agents. This process can be carried out either in-situ, in which the feed solution is replaced by the chemical agent, and the chemical solution is used as the incoming flow in the membrane module for membrane cleaning, or ex-situ, in which the fouled membrane is taken out and placed in a chemical solution tank for the rinsing process [6]. Proper chemical agents are required for each specific fouled membrane, depending on the type of foulant and chemical reaction between the foulant and chemical agents. Generally, temperature, pH, cleaning agent concentration, and the contact time play a significant role in cleaning efficiency [27]. The effectiveness of several cleaning chemicals on the membrane flux restoration was conducted by Li et al. [27]. Deionized water, NaOH, ethylene diamine

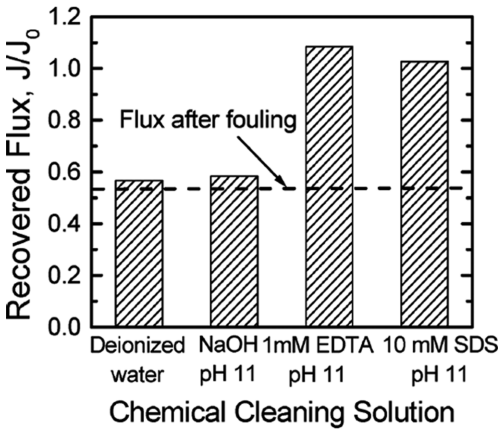

Fig. 5. Membrane flux recovery after using different chemical cleaning agents [27].

tetra acetate (EDTA), and sodium dodecyl sulphate (SDS) were applied to remove the organic fouling of a nanofiltration membrane. The result of the flux recovery is shown in Fig. 5.

It was reported that the cleaning efficiency of EDTA was strongly affected by pH, and the flux recovery with a cleaning solution pH of 11 was 35% more than the recovery at the ambient pH (approximately 4.8). It is worth mentioning that acids are the proper cleaning agents for inorganic fouling removal; however, alkalis are more useful for organic fouling mitigation. Thus, a combination of acid and alkali, used in rinsing the membranes, can detach most deposited foulants, and hence the permeate flux can be restored close to the initial value [88]. However, the main drawback to chemical cleaning is that the chemical agents can degrade the membranes. Other difficulties with this method are the chemical waste disposal, negative environmental impact, and excessive costs. Moreover, the most significant disadvantage of chemical cleaning is the decrease in the process productivity since the filtration system needs to be stopped for cleaning [6,68].

4. Biological Cleaning Method

A cleaning mixture of bioactive agents is utilized in biological cleaning processes to catalytically degrade the foulants and reduce the fouling propensity. The bioactive agents used in this method include antibodies, enzymes, peptides, polysaccharides, and nucleic acids [22,36]. Enzymes are considered as ideal agents since mild solution pH, temperature, and ionic strength are required for their interaction with other substances. Therefore, the use of bioactive agent does not degrade the membrane integrity and the membrane surface damage is not observed during the cleaning process [97].

The enzymatic treatment proved to be efficient for irreversible fouling mitigation. Allie et al. [98] employed lipases and proteases (enzymes) for fouling removal in a flat sheet membrane ultrafiltration of abattoir effluent containing proteins and lipids. The cleaning efficiency was determined based on the amount of proteins and lipids adsorbed onto the membrane as well as the pure water flux after the cleaning process. Lipase was proven to be a more effective agent, yielding a high cleaning efficiency and a low adsorption of particles onto the membrane. However, the combination of lipase and protease led to higher pure water flux. In another research, a commercial enzymatic detergent which is combined of proteases and anionic tensio-active was used for the cleaning process in whey proteins-feed ultrafiltration [99]. The cleaning efficiency was shown to be dependent on the experimental conditions, such as solution pH, enzyme concentration, cleaning time, and recycling versus no recycling of the permeate. Although residual matter was observed on the membrane, a cleaning efficiency of almost 100% was achieved only after 20 minutes of cleaning. Chen and Columbia [100] employed the enzymatic control method for alginate fouling of dead-end MF and UF ceramic membranes. Their finding showed a considerable effect of the enzyme, alginate lyase, on the fouling reduction. The fouling decline of 82% and 85% for MF and UF membrane was observed, respectively. It was also implied that a better flux recovery was obtained for the UF membrane with the enzymatic method since the alginate lyase had a high diffusivity, which was an essential factor for tight pores cleaning.

5. Membrane Surface Modification

Membrane surface modification is generally considered a fouling control strategy. Hydrophobic membranes are widely used in commercial applications regarding their excellent chemical, physical, and thermal stability. However, these membranes are more prone to fouling formation and have lower permeate flux compared with hydrophilic membranes. Therefore, the membrane surface modification is a viable control option in which the surface chemistry of the membrane is changed, and the membrane becomes hydrophilic with anti-fouling properties while the bulk properties are in their original conditions [18]. In order to change the membrane surface chemistry, modifying agents are employed either in the membrane preparation step (membrane polymer modification by copolymer blending or mixing the additives into the polymeric solution) or after the membrane fabrication (immobilization by grafting or solution coating). Among these methods, adding the modifying agent to polymer solution is less favorable due to particle aggregation in the dope solution, resulting in the reduction of the active surface area of additive particles. Moreover, a considerable part of the additives will deposit on the internal part of the membrane, which is not in contact with effluents [101].

For instance, the effect of polyethylene glycol (PEG) based copolymers on antifouling properties of membranes has been studied. Ding et al. [102] studied the surface grafting of a silicon rubber membrane by a series of di-block copolymers (PEG-b-cationic polycarbonates). They observed a great antifouling potential of PEG-*b*-cationic polycarbonates as a coating agent, as indicated by no biofilm formation after the surface modification by a particular polymer composition. Another study was also conducted on the antifouling properties of polyvinylidene fluoride (PVDF) as it was blended with PEG-based copolymers [103]. Although the blend and pristine PVDF membranes had a similar pore size, the hydrophilicity and antifouling propensity, as well as the final permeate flux of the blend membrane, were improved as the copolymers/PVDF blend ratio increased. A similar result was obtained by Sun et al. [104]. They worked on the hydrophilic modification of PVDF as an ultrafiltration membrane for the Bovine Serum Albumin (BSA) solution.

As mentioned, surface charge and surface roughness are also important considerations in fouling remediation. Membranes and foulants with a similar surface charge are less likely to lead to fouled membranes due to the electrostatic repulsive force between them. On the other hand, a smooth membrane surface is less susceptible to fouling formation. Therefore, surface modification is an appropriate method to change the surface properties by incorporating either the ionizable functional group or hydrophilic additives to reduce the fouling potential [105].

In summation, practically a combination of cleaning processes is employed to enhance membrane cleaning efficiency. For instance, most of the adopted physical methods are usually less effective compared to chemical cleaning. However, chemical methods are more likely to damage the membrane due to the chemical agent's existence. Thus, the physicochemical cleaning process appears to reduce the chemical agent loading as well as enhance the fouling reduction effectiveness. The chemically enhanced backwashing (CEB) is commonly used as a physico-chemical cleaning process. The result of a research conducted in Germany indicated that UF plants with regular CEB were required to use the chemical cleaning-in-place (CIP) method once every 1-5 years, while the plants without CEB were required to use CIP at least 1-4 times a year [6]. In addition, the combined method can be an effective way to remove both reversible and irreversible fouling, as compared with the use of each of the cleaning methods alone [106,107].

ULTRASOUND (US)-ASSISTED FOULING CONTROL

US irradiation could improve the filtration process efficiency without affecting the intrinsic membrane permeability. Ultrasonic waves are acoustic waves with a high-frequency range (higher than human hearing range of >20 kHz). These acoustic waves are capable of generating mechanical movement through a liquid medium [3]. US cleaning is an innovative and emerging strategy developed to overcome membrane fouling. It has been employed in various membrane filtration processes in order to break the concentration polarization or the cake layer on the membrane surface (Fig. 6) and can be applied to the processes either in-situ or ex-situ. US-assisted fouling control is a clean technique, alleviating the fouling potential via the cavitation bubble mechanism, since no chemical or biological agents are needed. In several recent studies, ultrasonic irradiation was applied to mitigate membrane fouling and recovery the permeate flux in a filtration process. Results of those studies indicated that US cleaning could be effective in improving the membrane capacity and filtration performance [108-116].

1. Mechanism of Microbubble Cavitation on Fouling Removal

Intense ultrasonic pressure cycles between compression and rarefaction results in bubble formation. Cavitation is described as the bubble formation (nucleation), growth, and its collapse in an aqueous solution. Cavitation exerts a high drag force on the accumulated particles and removes them from the membrane surface. Bubble collapse and bubble oscillation on the membrane surface play an important role in the cleaning process [118].

Liquid molecules are subjected to positive and negative pressure during US irradiation. During the compression cycle with a positive acoustic pressure the molecules are forced close to each other, while during the rarefaction cycle with a negative acoustic pressure, the molecules are pulled apart. During the rarefaction cycle, as the created tensile stress created by the negative acoustic pressure becomes greater than the liquid tensile strength due to the intermolecular force between molecules, cavitation bubbles are formed. The required acoustic pressure to initiate cavitation is higher in a pure liquid since the liquid tensile strength decreases remarkably in the presence of impurity or a dissolved gas in the liquid [3]. The created bubbles, known as cavities, can be empty or filled with vapor or dissolved gases [11]. During the rarefaction cycle, a pressure reduction to below the vapor pressure of the liquid brings about the formation of the nano and microbubble nuclei. The growth of created cavities is caused by two phenomena, coalescence and rectification. The combination of small cavities to form larger bubbles and bubble growth under frequent compression and rarefaction cycles is known as coalescence and rectification, respectively. Liquid vapors and dissolved gases enter or leave the cavities during the US propagation, and the amount of exchanged gas/vapor depends on the bubble surface area. Therefore, during the rarefaction cycle, owing to the larger bubble surface are under this cycle, the amount of material penetrating the cavities is higher than the amount of material discharged from the bubbles during the compression cycle [11]. The bubbles keep growing through several compression-rarefaction cycles and reach a maximal radius and, consequently, bubble implosion occurs. Generally, the bubble collapse generates a considerable chemical and mechanical energy in an aqueous solution. The transferred energy from bubble collapse to the membrane surface and the formation of a high local stress bring about the foulant removal [11,118-120]. The creation of acoustic cavitation and cavity growth as well as the cavity explosion are shown in Fig. 7.

During the US irradiation of a liquid, acoustic streaming, microst-

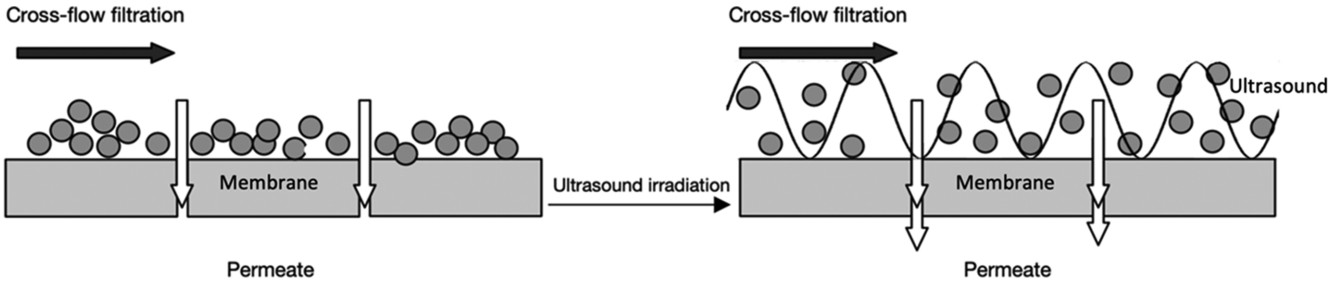

Fig. 6. Schematic diagram of flux enhancement via US irradiation [117].

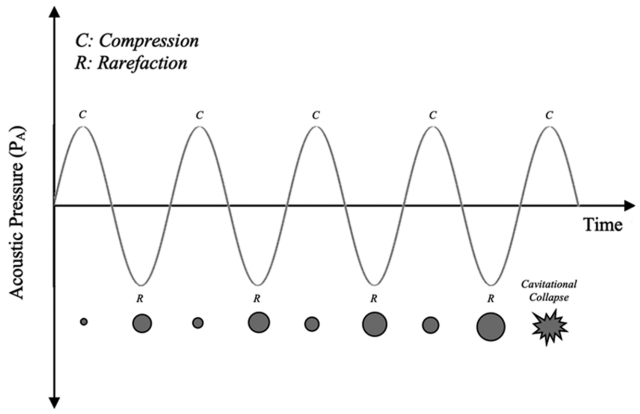

Fig. 7. Schematic diagram of acoustic cavitation creation, cavity growth, and cavitation explosion [3].

reaming, micro-streamers, micro-jets, and shock waves are created in the liquid. These physical phenomena are able to dislodge the attached particles from a solid interface in contact with the liquid [3].

Acoustic streaming is the result of acoustic energy absorption in the liquid, and its effective range is on the order of centimeter to tens of centimeters. This phenomenon can take place without bubble explosion and is more favorable for the removal of the relatively weak fouling layer containing dissolvable particles. During acoustic streaming, the water molecules are circulated frequently in a back and forth motion, which causes a fluid velocity gradient near the membrane surface and results in particle detachment [121]. Acoustic streaming is more efficient in a dead-end filtration than in a cross-flow filtration process [11].

Microstreaming takes place when the cavitation bubbles oscillate to create fluid circulation. Fluid circulation and liquid molecules replacement causes a rapid eddy current and shear force as well as a dynamic velocity profile applying drag forces on the attached particles and removing them from the solid surface. As previously mentioned, higher US frequency leads to smaller bubble size and eddy current while more microstreaming is generated at lower US frequency irradiation [121]. Microstreaming near the solid boundary is effective for foulant remediation [122].

Micro-streamers are defined as cavitation bubbles moving towards the antinodes in a torturous path and create a ribbon-like structure [121]. The antinodes are created by means of the reflected US wave from a solid surface and the incoming US wave from a transducer. According to the Bjerknes forces, antinodes of the standing waves adsorb cavitation bubbles smaller than resonance size, while bubbles larger than the resonance size are attracted by nodes. Microstreamers dislodge the attached particles as the antinodes on the membrane surface adsorb the cavitation bubbles [3].

Micro-jets are generated as a result of asymmetric bubble explosion. During US irradiation, cavitation bubbles move toward the membrane surface and get close to the solid boundary. At this

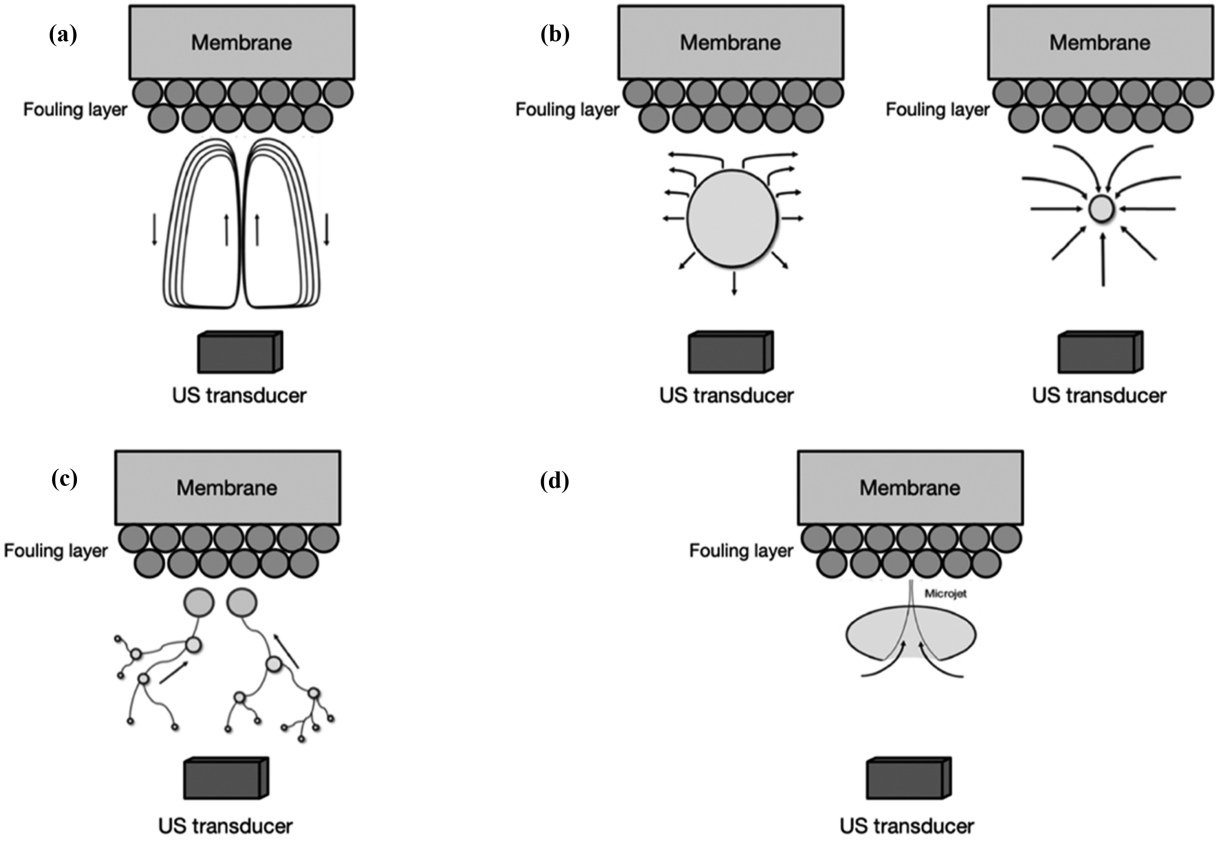

Fig. 8. Schematic representation of the produced physical phenomena via US irradiation, (a) acoustic streaming, (b) microstreaming, (c) micro-streamers, (d) micro-jets [3].

instance, fluid movement around the bubble decreases and results in differential pressure and loss of spherical geometry of cavitation bubbles. As the differential pressure becomes large enough, bubble explosion occurs and causes a high-speed liquid microjet formation, which is able to clean the clogged surface [3,123]. All the proposed mechanisms are depicted in Fig. 8.

Shock wave formation is also among the important mechanisms for membrane fouling control. This mechanism takes place as a result of the collapse of the cavitation bubbles. The bubble collapse produces high pressure cores, resulting in high pressure (more than 10 kbar) shockwaves directed toward the solid interface [123].

The energy within the cavities before the explosion can be determined as follows [124]:

$$W_{Cav}=\frac{4\pi R_{rs}^3}{3}P_0 \tag{42}$$

where P_0 is the hydrostatic liquid pressure and R_{rs} is the resonance frequency.

The critical size of the cavitation bubble, known as the resonance size, depends on the US frequency according to the following equation [3].

$$R_{rs}=\frac{1}{2\pi f}\left(\frac{3kP_0}{\rho}\right)^{1/2} \tag{43}$$

where, f is the US frequency, k the polytropic coefficient, and ρ the liquid density.

Kanthale et al. [125] and Gogate et al. [126] observed that the cavitation bubbles were presented in the form of clusters, and the collapse of a single cavity influences the dynamic of the surrounding cavities. Therefore, the active volume of the cavitation bubble (V_{Cav}) and the collapse pressure (P_C) generated can be expressed by the following equations [125]:

$$V_{Cav}=(4{\cdot}39\times10^{-4})(P_s)^{1{\cdot}3342}(I)^{0{\cdot}264}(R_0)^{2{\cdot}728}(f)^{-0{\cdot}021}(\theta)^{0{\cdot}1} \tag{44}$$

$$P_C=(0{\cdot}0159)(I)^{0{\cdot}330}(R_0)^{-0{\cdot}134}(f)^{-0{\cdot}042}(\theta)^{0{\cdot}634}(R/R_0)^{-2{\cdot}969} \tag{45}$$

where P_s is the threshold pressure of the active zone of cavitation, I the US power intensity, R_0 the initial cluster radius, f the US frequency, θ the fraction of energy transfer, R the maximum cluster radius. The radius of a single bubble was assumed to be 1×10^{-6} m.

Eqs. (44) and (45) are applicable within the range of the parameters as follows:

$I=50-250\times10^4$ W/m^2
$R_0=0.5\times10^{-3}-5\times10^{-3}$ m
$f=20\times10^3-300\times10^3$ Hz
$\theta=0.25-0.45$

The wall velocity of the cluster (S_c) during the bubble explosion can be calculated as below [125]:

$$S_c=\left[\frac{P_c}{\rho\beta(1-\beta)}\right]^{1/2} \tag{46}$$

where β is the void fraction of the cluster.

The velocity induced by the bubble explosion imparts a flow toward the membrane surface, which creates shear stress on the solid interface, and in turn, results in foulant detachment. In fact, the velocity is one of the key factors influenced the dislodgment of the adhered foulant. The shear stress created by the collapse of the cavity cluster close to the membrane surface, can be expressed as follows [124]:

$$\sigma_C=\frac{\mu S_c}{\delta_f} \tag{47}$$

where μ is the dynamic viscosity of the liquid and δ_f the fouling layer thickness.

The flow velocity and pressure induced by the cavity cluster explosion can also cause membrane erosion. Bedkowski et al. [127] proposed an equation for erosion stress (σ_{EROS}) of the membrane surface as a function of the collapse pressure.

$$\sigma_{EROS}=E{\cdot}P_C \tag{48}$$

where E is the erosion susceptibly constant and can be expressed by the following [124,127]:

$$E=1-\left[\left(\frac{H_m}{H_d}\right)\left(\frac{F_{g.min}}{F_m}\right)\left(\frac{1}{10R_a}\right)\right] \tag{49}$$

In this equation, the subscripts d (diamond) and g (glass) represent reference materials for hardness (H) and fragility (F), respectively. The subscript "m" refers to the clean surface of the material, and R_a is the arithmetic roughness. Therefore, for the materials with a soft, fragile, rough surface, the erosion susceptibility constant is almost unity, and it becomes smaller as the surface changes to a hard, ductile, smooth condition.

Unlike the particle-shearing stress, which results in fouling dislodgment, the erosion stress on the membrane surface imparts more particles. Thus, the net cleaning ability of the sonic field can be determined as the difference between particle-shearing stress and erosion stress.

$$\sigma_{Clean.Cav}=(\sigma_C-\sigma_{EROS})=\frac{\mu}{\delta_f}\left[\frac{P_c}{\rho\beta(1-\beta)}\right]^{1/2}-E\cdot P_C \tag{50}$$

Thus, the net cleaning force can be rewritten as follows:

$$\sigma_{Clean.Cav}=AP_c^{1/2}\text{-}E{\cdot}P_C \tag{51}$$

As evident in this proposed model, the foulant dislodgment was limited to the cavitation bubbles and the shearing stress induced by the cavity cluster explosion. At the same time, acoustic streaming also has a pivotal role in the cleaning process. Further discussion regarding the effect of acoustic streaming on fouling removal is also dealt with in the following section. The velocity of acoustic streaming is determined as [127]:

$$S_{Ac}=2\varphi I(2a)^2/\mu c_s \tag{52}$$

$$\varphi=2\mu f^2/(3\rho c_s^3) \tag{53}$$

where φ is the absorption coefficient, 2a the beam width, and c_s the sound velocity.

The total flow velocity and shearing force exerted to the fouling layer, which caused the particle detachment from the extent surface, is the sum of the flow velocity and shear stress induced by cavity cluster explosion and acoustic streaming. Note that despite the cavity cluster explosion, acoustic streaming does not contrib-

ute to surface erosion (σ_{EROS}=0). Therefore, the total flow velocity (S) and cleaning ability (σ_{Clean}) can be expressed as follows [124]:

$$S=\left[\frac{P_c}{\rho\beta(1-\beta)}\right]^{1/2}+8\varphi I a^2/\mu c_s \quad (54)$$

and

$$\sigma_{Clean}=AP_c^{1/2}-E\cdot P_C+8\varphi I a^2/\delta_f c_s \quad (55)$$

Ultrasonic irradiation can create significant physical phenomena in the liquid, which eventually breaks the cake layer and prevents particle deposition on the membrane surface. The effectiveness of the generated sound waves on fouling removal depends on several parameters, such as US frequency, power intensity, temperature, pressure, US irradiation mode, US transducer position, cross-flow velocity, and feed solid concentration. The effective parameters that influence the effectiveness of US irradiation are summarized below.

2. Effective Parameters in US Performance

2-1. US Frequency

Generally, US frequencies between 20 kHz-100 kHz are used in experiments on membrane fouling control. In this range, lower ultrasonic frequencies were proven to be more efficient in mitigating membrane fouling regardless of membrane materials and types [22]. The cavitation bubble diameter and energy released during its explosion is inversely proportional to the US frequency [3,128, 129]. A higher US frequency leads to smaller cavitation bubbles and a greater US attenuation, which results in reduction in cleaning efficiency [22]. Although the number of produced bubbles increases at a higher US frequency, the cavitation bubbles are not capable of creating a highly turbulent flow. In fact, at a higher US frequency, the cavitation bubble size is smaller and, hence, both the acoustic cavitation and bubble explosion occurs less violently and without sufficient energy for breaking the concentration polarization or pitting and eroding the fouled layer [3,11].

Kobayashi et al. [128] investigated the effect of the US frequency on filtration treatment of peptone and milk solution with UF and MF membranes, respectively. They employed three different frequencies of 28, 45, and 100 kHz and reported that the permeate flux for the peptone solution filtration was improved by more than 20% as the frequency was decreased from 100 kHz to 28 kHz. A similar increasing trend of the permeate flux with decreases in the frequency was observed for MF treatment of the milk solution where the volumetric flux increases from 3×10^{-5} to 9×10^{-5} $m^3/m^2\cdot s$ were found. Lamminen et al. [121] observed an increase in the permeate flux as the frequency decreased from more than 1,000 kHz to less than 10 kHz. Kyllönen et al. [130] noticed a minor effect when the US frequency of 200 kHz was used, and a similar result was observed as they changed the US frequency from 200 kHz to 27 kHz at the input power of 200 W. The influence of US frequency on reversible fouling (as the dominant fouling resistance) of *Radix Astragalus* aqueous extract (natural product) was also studied by Cai et al. [131]. The authors reported that although the reversible fouling was reduced by 40% at US frequencies of 28 kHz and 45 kHz, the cleaning efficiency reached almost zero as the US frequency was increased to 100 kHz.

Cai et al. [7] also observed the permeate flux enhancement of 10% and 27% under the US frequency of 100 kHz at 360 W and 600 W, respectively. As the frequency was decreased from 100 kHz to 45 kHz, similar flux enhancement values (11% and 28%) were obtained at 30 W and 90 W. Therefore, it was concluded that lower frequency is more efficient not only for its desirable fouling mitigation but also for its low power consumption. Heikkinen et al. [132] showed the effect of the US frequency on the reduction of the concentration polarization. They observed a remarkable water flux enhancement which was nearly two-fold with the use of the US frequency at 20 kHz. However, the results were not favorable at high frequencies. Similar results on the effect of the US frequency on the cleaning efficiency and permeate flux improvement were also reported by Lujan-Facundo [133].

2-1-1. Mixed Wave Mode

Mixed wave mode, using different US frequencies (low and high frequencies) in tandem, is a simple method employed for the removal of membrane foulants. Gonzalez-Avila et al. [134] employed a high US frequency of 220 kHz, which was exerted on the system in order to create the cavitation bubbles, followed by a low frequency of 28 kHz to excite the microbubbles. The membrane flux and the transmembrane pressure were analyzed to evaluate the US performance. Their findings showed a high recovery of the transmembrane pressure (almost complete restoration) and a membrane flux improvement. The high US frequency was applied first to the system to nucleate more bubbles close to the membrane interface. Those small bubbles did not have sufficient energy to break the cake layer or prevent the particle deposition. Thus, the driving sound field was switched to the lower frequency under which condition the bubble radius increased, resulting in a violent bubble collapse and shock waves as well as high turbulence and shear force. Although the tandem frequency proved was shown to be efficient for the transmembrane pressure recovery and the flux enhancement, the effect of this method on the membrane integrity needs to be addressed. Similar findings were obtained by Alventosa-deLara et al. [13] and Maskooki et al. [135] for mixed US frequencies of 37 kHz and 80 kHz.

2-2. Power Intensity

Sound energy is measured by the power intensity, defined as the amount of energy output per second per unit area of a US transducer. Power intensity enhancement results in a more intense sonochemical effects. In fact, when the power intensity is increased, more cavitation bubble and larger cavitation zone are created owing to a higher acoustic pressure amplitude [11]. Eq. (56) presents the relationship between the US power intensity and the acoustic pressure amplitude [3].

$$I=\frac{P_A^2}{2\rho c_w} \quad (56)$$

where I is the power intensity, P_A is the acoustic pressure amplitude, and c_w is the speed of the US wave.

In addition, a high-power intensity enhances hydrodynamic turbulence since the bubble collapse intensity and the acoustic energy absorption increase under a high-power condition. Therefore, a high US power leads to permeate flux enhancement and less particle deposition on the membrane surface and, hence, a high permeate flux [121]. Cai et al. [131] tested three different US powers

of 60 W, 90 W, and 120 W and observed permeate flux increases of 35%, 57% and 68%, respectively. A similar result was obtained by Zhang et al. [1]. The permeate flux enhancement of 12%-15% to nearly 70% was reported with the power intensity increases from 10 W to 120 W. The foulant rejection was also increased under the US irradiation. Similar results were obtained by Lamminen et al. [121], Maskooki et al. [135], Matsumoto et al. [136], Kobayashi et al. [137], Juang et al. [138], Muthukumaran et al. [139], Mirzaie and Mohammadi [140], and Kan et al. [141].

Nevertheless, extremely high power density may affect the membrane integrity and result in membrane damage [22]. More recently, Thombre et al. [9] worked on the US cleaning of a nanofiltration membrane. Although a significantly positive effect of the high-power intensity on the flux recovery and the fouling mitigation was achieved, membrane damage was observed at the US power of 150 W. Aside from membrane integrity, the power intensity beyond a critical value also results in a high energy consumption that is not favorable in industrial applications. Thus, an optimal power intensity is required to reach a maximal level of permeate flux and fouling removal without any negative effect on the membrane structure and a massive energy consumption.

2-3. Temperature

Increasing the liquid temperature results in lower liquid viscosity and surface tension of the liquid medium [142]. Moreover, contaminant solubility in liquid, especially for liquids used in the dairy industry, may increase with temperature. Thus, dissolution and back diffusion of the dairy contaminant to the bulk solution increase with temperature, resulting in a cleaning efficiency improvement. Chai et al. [143] investigated the effect of temperature on the performance of a US-assisted filtration process with a peptone solution. According to their findings, the permeate flux was improved when the temperature was increased from 20 °C to 40 °C. The flux improvement was the result of the liquid viscosity decrease, caused by increasing the temperature. The flux recovery also seemed to be faster and increased rapidly under higher temperatures owing to the higher solubility and back diffusion of the fouled peptone to the aqueous solution. Similar result was obtained by Muthukumaranet al. [139].

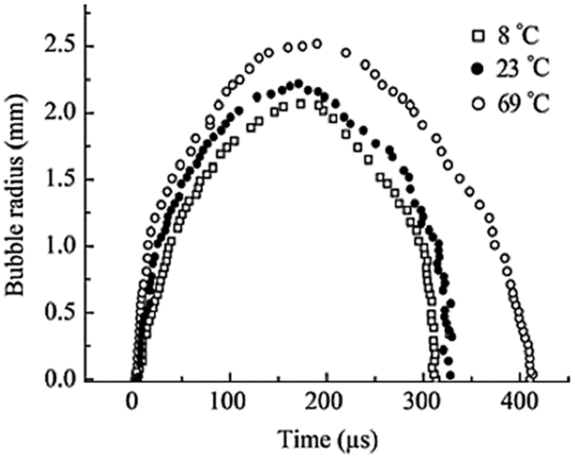

Fig. 9. The bubble radius and lifetime in distilled water at three different temperatures [146].

Increasing the liquid temperature seems to have a positive effect on the maximum bubble radius, as well as the bubble lifetime [144]. Fig. 9 shows the bubble radius and lifetime of a laser-induced single bubble in distilled water at three different temperatures. However, as the temperature is raised, the vapor pressure also increases. Higher vapor pressure affected the bubble dynamic significantly and led to less intensive shock-wave created during the bubble collapse [145].

Zhu et al. [145] reported that the permeate flux improvement of a US-assisted membrane distillation process was reduced at higher temperature conditions. The decreasing trend of the permeate flux was attributed to the higher vapor pressure. A similar result was also reported by Li et al. [147] who used ultrasound to clean membrane in microfiltration of pulp and paper effluents. Their observation indicated that the cavitation effectiveness was decreased (not intensive shock waves) when the temperature was increased from 23 °C to 40 °C and, in turn, that led to the decreases in the permeate flux recovery.

To maximize the cleaning efficiency and filtrate flux recovery, an optimal temperature is necessary. Wang et al. [148] studied the effect of temperature on the US-assisted cleaning of membrane used in nanofiltration of a solution containing inorganic materials. They showed that flux recovery increased as the temperature was increased from 15 °C to 30 °C. However, a further increase in temperature beyond 30 °C resulted in a sharp decline of the flux recovery. This indicates that the maximal efficiency was attained at 30 °C.

2-4. Pressure

Liquid pressure can affect both the cavitation bubbles and particle deposition behavior on the membrane surface. An increase in liquid pressure causes an increase in the bubble-generation threshold pressure and compressive forces driving the bubble collapse, which in turn results in formation of fewer bubbles but with more intense bubble explosion. High compressive forces increase the velocity of the bubble wall during the bubble explosion. Therefore, more substantial turbulence flow and shear force are generated due to the more vigorous cavitation bubble collapse in the vicinity of the membrane surface, which leads to the foulant dislodgment and surface cleaning improvement [15,149]. From the particle deposition point of view, an increase in filtration pressure may cause a significant increase in the permeate drag force on the foulant particles at the membrane surface due to an increase in the permeate velocity, as indicated by Eq. (57) below, which results in more fouling. Assuming that foulants are spherical particles, the permeation drag force can be expressed as follows [15]:

$$F_D = 3\pi\mu a_p v \quad (57)$$

where a_p is the particle diameter and v the permeate velocity.

In addition, increasing the applied pressure results in more compact fouling formation since foulants are forced into membrane pores and compressed further against the surface. Therefore, increases in pressure, along with US irradiation which caused particles dislodged and moved back to the bulk solution, could force the dislodged particles to reattach to the membrane surface again [13,139]. Chen et al. [15] evaluated the effect of the filtration pressure on ultrasonic fouling control in ultrafiltration of silica colloids

by a ceramic membrane. An ultrasonic probe was placed parallel to the membrane surface in a cross-flow filtration membrane module. They observed a decreasing trend in the relative permeate flux improvement (100% to 59%) as the filtration pressure was increased from ~0.07×10^5 Pa to 0.54×10^5 Pa. The relative permeate flux improvement is defined as the ratio of the difference between the steady-state permeate flux of fouled membrane with US and without US to the difference between the permeate flux of clean membrane with US and the flux of fouled membrane without US. As the pressure is increased, the permeate velocity through the membrane also increase. Therefore, according to Eq. (57), the permeate drag force on deposited particles also increases and causes more severe particle adhesion on the membrane surface. Consequently, the relative permeate flux improvement decreases with pressure. Nevertheless, the actual permeate flux could increase by more than three-fold as the pressure is increased. According to the decreasing trend of the relative permeate flux improvement with the filtration pressure, it can be concluded that the effect of the permeate drag force is more dominant than that of the increase in the intensity of bubble explosion or acoustic streaming.

The effect of the TMP on the performance of US-assisted cleaning of fouled ultrafiltration membrane was studied by Alventosa-deLara et al. [13]. The membrane unit was submerged in an ultrasonic bath. The US cleaning experiments were carried out with a cross flow of deionized water at different TMP of 0.5×10^5 Pa, 1.5×10^5 Pa and 2.5×10^5 Pa in the membrane unit. The best cleaning efficiency was obtained at the TMP of 1.1×10^5 Pa. Further increase in TMP led to more decay in the surface cleaning efficiency. TMP increase between 0.5×10^5 Pa to 1.5×10^5 Pa resulted in a stronger cavity explosion and acoustic streaming. Therefore, turbulence flow and shear forces created in the bulk liquid and the vicinity of the membrane surface could overcome the permeate drag forces and dislodge the particles. Kyllönen et al. [130] also investigated the effect of the TMP on the efficiency of the US-assisted filtration process with the US traducers placed on the membrane module. It was observed that the contaminants fouled the membrane severely at the high-pressure conditions; thus, the surface cleaning was more difficult.

In fact, pressure can have various effects on membrane cleaning and flux enhancement. The cleaning efficiency and the permeate flux may vary (increase or decrease) under the pressure increase and US irradiation owing to the pressure altering range, the US transmitting properties, foulant characteristics and membrane chemistry.

2-5. US Radiation Mode (Pulsed/Continuous)

US irradiation can take place in either continuous or intermittent (pulsed) mode. In the pulsed mode of US irradiation, different off intervals (US deactivation) are applied between US irradiation cycles, which leads to the reduction of energy consumption. Moreover, pulsed irradiation may prevent membrane damage at high US power intensities. Chen et al. [15] studied the effect of continued/pulsed US irradiation on the relative permeate flux improvement of a cross-flow, flat sheet membrane system. The filtration system was a cylinder with an ultrasonic probe located above the membrane. Different pulse interval (0.1 s, 0.3 s, 0.5 s, 1.0, and 2.0 s of US deactivation) were used between 1.0 s of US irradiation. A relative permeate flux improvement of nearly 75% was obtained with the continuous US mode, and it decreased to almost 27% with pulsed US at 2.0 s interval (1.0 s on/2.0 s off), as compared with that without US application. Thus, it was suggested that the ultrasonically generated turbulence flow slowly faded, and more particles tended to accumulate on the membrane surface when the pulsed US was applied to the system. Aside from the flux improvement, the energy consumption at a very short pulse interval (0.10 s US deactivation) was almost 9% less than that for continuous US, while its cleaning effect was so close to that of continous mode (nearly 73% improvement over that without US).

Cai et al. [131] used continuous US irradiation and three different intermittent modes (on-off duration: 1-1 s (A), 1-5 s (B), and 1-9.9 s (C)) to clean the fouled membrane in a UF cell. The stirred UF cell was placed in a US bath. The filtration resistances were measured, and it was observed that the resistance increased as the US irradiation changed from continuous mode to the intermittent mode and this increasing trend continued as the US on/off duration ratio decreased. The permeate flux at the "B" and "C" mode, as referred to above, was almost similar and lower than that of the "A" mode (40% lower). Although continuous US irradiation seemed to be more effective in fouling mitigation and flux improvement, the "A" mode was chosen as an efficient US intermittent cleaning since it is an economically viable process, under which the membrane maintained its integrity. Similar results on flux decay by increasing the time interval in intermittent mode were reported by Lee et al. [17].

Kan et al. [141] investigated the effect of pulsed US irradiation on natural organic matter fouling removal. The results showed that as the on US cycle was reduced from 9 s to 3 s irradiation, the relative permeability decreased from 49.4 to 25 (almost 48% reduction). It was also mentioned that although cleaning efficiency is always higher with the continuous US mode, pulsed US irradiation results in a lower power consumption, and hence a more energy-efficient cleaning process. Yu et al. [150] observed a similar trend of cleaning efficiency for the pulsed mode as they increased the US irradiation period from 3 min to 10 min. Mirzaie and Mohammadi [140] also assessed the effect of pulsed US irradiation (on-off duration: 0.8-0.2 s) on the cleaning efficiency and the flux recovery of MF membrane using a milk solution as a feed. It was reported that although the steady-state flux was 33% lower than that with the continuous mode, the energy consumption was lowered by almost 20%. Finally, the most effective radiation mode may vary, depending on the type of membrane and feed properties [7,15].

2-6. US Transducer Position

Chen et al. [15] studied the effectiveness of the US source position on the performance of a US-assisted filtration process. The distance between the membrane module and the US probe was chosen to be 3.5 cm, 2.6 cm, and 1.7 cm. It was found that the smaller distance was more effective in improving the relative permeate flux. For larger particles (1.56 μm), as the distance was decreased from 3.5 cm to 2.6 cm and 1.7 cm, the flux increased by 60%, 75%, and 97%, respectively. However, fouling control was less effective with smaller particles (0.22 μm) where the relative flux improvement was only 29%, 30%, and 59% at similar distances. This finding was attributed to the attenuation of the propagated sound

intensity. As the distance from the US source to the membrane decreased, stronger sound waves reached the membrane surface and resulted in more turbulent flow, which facilitated a better removal of foulant and hence flux improvement. A similar result was reported by Lujan-Facundo et al. [14]. They placed the US transducer at the bottom of a US tank and submerged a membrane module inside the tank. Two positions of the membrane unit were investigated: at the bottom of the tank (distance of 0.0 cm from the US transducer) and 3.0 cm above the bottom of the tank. The results showed a slightly higher cleaning efficiency with the former membrane position.

Mirzaie and Mohammadi [140] also employed US irradiation to facilitate fouling removal in microfiltration of a milk solution. They observed that as the distance between the US probe and the membrane module got larger from 2.6 cm to 4.4 cm, the permeate flux recovery was reduced from 228% to 145%. Also, membrane damage (cracks at the center of membrane area) was observed at a distance of less than 2 cm. As a result, although the cleaning efficiency and the membrane permeate flux increased with shorter distances, membrane damage could occur when the membrane module is too close to the US source. In fact, at a very close distance, energy density is extremely high and all the possible mechanisms (micro-jet, microstreaming, micro-streamers, acoustic streaming, and shock waves) may contribute to the membrane cleaning process [15,151].

2-7. Feed Concentration

Generally, membrane flux is inversely proportional to the feed solid/foulant concentration regardless whether filtration is with or without US irradiation. However, in the case without US irradiation, the flux decline with a high concentration of feed is more severe. US irradiation was shown to be effective in enhancing the permeate flux of dairy solutions even at a high solute/foulant concentration. However, the permeate flux of the whey solution decreased with increasing the feed concentration [139]. Feed solution with a high particle concentration can readily increase the viscosity, and hence reduce the probability of cavitation bubble production within the solution. Thus, larger acoustic pressure is required to overcome the natural cohesive forces of liquid molecules so to create voids or cavities [11]. Chen et al. [152] reported that the permeate flux restoration decreased from 100% to 65% as the feed silica oxide concentration was increased from 0.5 g/L to 1.8 g/L, using a membrane module and a US source at 1.7 cm apart. It also was shown that US irradiation was more efficient at a low feed concentration. In fact, higher feed concentration results in a greater acoustic impedance, which leads to a significant sound wave attenuation [11]. Additionally, the interaction of the particles also increases in this case, which may affect the US performance on the foulant removal and the flux enhancement. It was noted that the sound wave intensity was absorbed and scattered by cavitation bubbles. In this regard, the wave intensity, reflected by the equilibrium temperature difference of the solution between the initial stage prior to the sonication and during the sonication, was measured at different feed concentration to evaluate the effect of particle concentration on sound absorption as well as sound scattering, which resulted in lower fouling mitigation. Fig. 10 shows that the wave intensity was reduced with the particle concentration at the cavitation region (at 1.5 cm distance from US source). In fact, particles acted as nuclei and caused additional cavitation bubble generation near the US sources, which resulted in sound wave attenuation and propagation impedance due to the scattering and absorption [152].

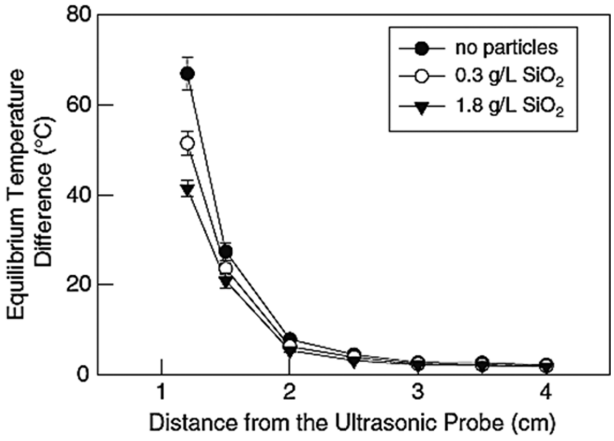

Fig. 10. Sound wave intensity as function of particle concentration during the US radiation [152].

In addition to the particle concentration in the feed stream, the particle size also has a substantial impact on the fouling layer formation. Mah et al. [153] reported that smaller components tend to form a denser fouling layer on the membrane surface, which leads to a higher resistance and further permeate flux reduction. A similar result was also revealed by Lim and Bai [33].

3. Combination of US with other Cleaning Techniques

US cleaning is an effective method for pitting and eroding the deposited particles and the reversible cake layer from the membrane surface. However, irreversible fouling maintains after the US irradiation and other cleaning methods (mostly chemical cleaning) are required to overcome this problem. In this regard, the combination of the sonication technique with other cleaning methods is employed in order to increase the cleaning efficiency, reduce energy consumption, and minimize the utilization of chemical agents.

As mentioned, physical cleaning may be considered less effective than chemical cleaning. However, using physical cleaning such as forward flushing, back flushing, gas sparging and hydraulic washing under the US irradiation can facilitate cake layer removal [147]. Li et al. [147] worked on the permeate flux recovery by US cleaning, forward flushing, and US-associated forward flushing of fouled nylon membrane. The permeate flux of membrane fouled with DAF product from paper industry was 52.8 l/m^2h; and the flux increased to 86.4 l/m^2h after washing fouled membrane with water. On the other hand, the permeate flux reached 122.41 l/m^2h and 350 l/m^2h by forward flushing and sonication, respectively. Eventually, as forward flushing was employed under the US irradiation, the permeate flux further increased to 738 l/m^2h, which was only 18% lower than the initial pure water flux. Similar results were reported by Lee et al. [154] when they used sonication and flushing as well as their combination for membrane cleaning. Shahraki et al. [155] investigated the effectiveness of gas bubbling on the flux improvement in a US-assisted ultrafiltration of a 1%

skimmed milk feed solution. An ultrafiltration unit was submerged in a US bath. It was reported that the membrane flux improvement was about 72% and 180% by gas bubbling and US irradiation, respectively. Moreover, the membrane flux increased further to 384% when the combination of sonication and gas bubbling was applied to the filtration process.

The combination of chemical cleaning with US irradiation was studied by Muthukumaran et al. [156]. An anionic detergent was used in combination with sonication for foulant removal from an ultrafiltration membrane fouled with a dairy product. It was reported that chemical cleaning and US acted synergistically and the flux increased significantly. For a fouling time of 20 min and sonication cleaning time of 20 min, the flux improvement was between 25% to 41%. However, under the combination of sonication and chemical solution, the flux increased to 150%. A similar result was demonstrated by Maskooki et al. [157] who investigated the combined effect of EDTA and US irradiation in cleaning microfiltration membrane (milk was used as feed solution). Most recently, Thombe et al. [9] showed that the use of NaOH, as a chemical cleaning agent, under the US irradiation, increased the cleaning efficiency and flux recovery to almost 90% in 4 min. The ability of ultrasound cleaning technique for irreversible fouling removal was studied by Lujan-Facundo et al. [133]. Ultrasound irradiation was employed in combination with chemical cleaning (NaOH solution) after an initial rinse with distilled water. As mentioned, chemical cleaning is the most favorable method for breaking the severe and irreversible fouling layer. It was reported that the membrane flux recovery improved by 10% by using the US irradiation with chemical cleaning. This shows a promising result as to the ability of US cleaning for irreversible fouling mitigation.

4. Highlights, Challenges and Future Outlook of US Cleaning

First and foremost, an important advantage of the in-situ ultrasonic irradiation is that the filtration process is not interrupted by the cleaning process as the case for physical, chemical or biological cleaning methods. Thus, using US cleaning prevents system downtime and improves filtration efficiency. US irradiation can be carried out automatically and simply combined with other methods to achieve desirable fouling removal and permeate flux im-

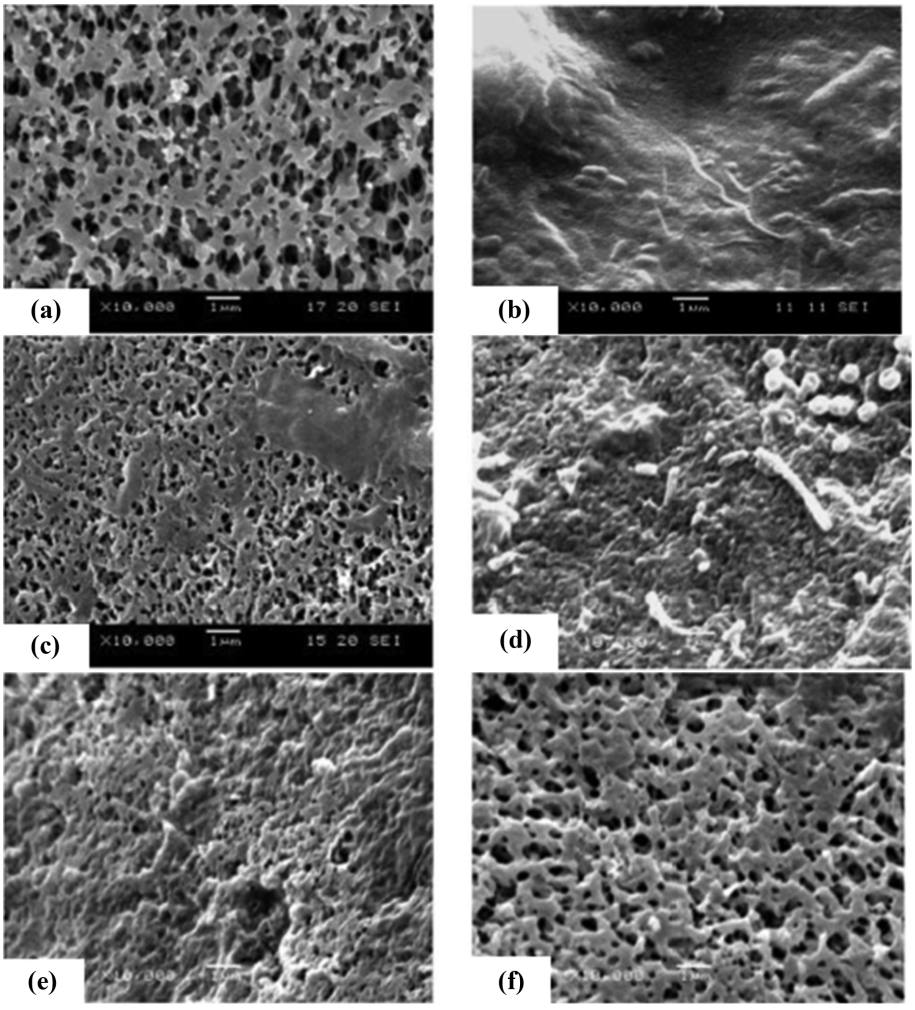

Fig. 11. The SEM image (image magnification of 1 mm) from the surface of (a) neat membrane, (b) fouled membrane, (c) fouled membrane under sonication, (d) fouled membrane cleaned by backwashing, (e) fouled membrane cleaned by chemicals, (f) fouled membrane cleaned by combined method [33].

provement. In addition, US-assisted fouling control processes avoid chemical use and chemical disposal, which results in minimization of environmental impact and improving the membrane lifetime as well as reducing the operating costs. Besides, ultrasonic irradiation was shown to be a less energy-intensive method (energy saving), in which little labor is required. Therefore, the use of US cleaning leads to lower operating cost in large-scale applications compared with other cleaning methods. According to Lujan-Facundo et al. [158], only 19% of the daily cost in a membrane cleaning process (chemical cleaning plus US cleaning) was related to US cleaning. Therefore, it can be concluded that the US cleaning process is an economically viable method for fouling mitigation.

To compare the US cleaning efficiency to other cleaning methods, Lim and Bai [33] used sonication to clean a fouled membrane in microfiltration of activated sludge and evaluated its efficiency by measuring the permeate flux recovery. The result of their study was compared with membrane cleaning by water backwashing and chemicals as well as the combination method (sonication followed by water backwashing and chemical agents). The SEM images from the surface of the clean membrane, fouled membrane and membranes after individual cleaning methods are given in Fig. 11. According to their findings, the combined cleaning was the most effective method giving an almost complete flux recovery (95.7%), followed by chemical cleaning (76.8%), sonication for 10 min (60.8%) and deionized water backwashing (24.7%). As SEM images reveal, US irradiation removed most of the cake layer and deposited particles on the membrane surface by breaking down the cake layer, which resulted in permeate flux enhancement (Fig. 11(c)). However, foulants and cake layer can still be seen on the membrane surface after chemical cleaning (Fig. 11(e)). Chemical cleaning increased the flux recovery by increasing the attached biofilm permeability. In fact, chemical cleaning was more effective for adhesive fouling causing the biofilm attachment within the pores or on the membrane surface. Water backwashing was not effective for this system, and only a small part of the foulants (loosely attached particles) was removed from the surface or membrane pores (Fig. 11(d)). The combined method was found to be the most efficient process for fouling removal and flux improvement. As shown in Fig. 11(f), the membrane surface is clean and porous.

Aside from the strength of this novel and viable cleaning method, several issues regarding the effect of US waves on the membrane integrity and its weakness on the pore blockage fouling removal should be considered. As mentioned, this method is not favorable for the elimination of irreversible fouling and needs to be used simultaneously with other cleaning techniques to remove the gel layer or foulant within the pores. Moreover, US irradiation may increase the particle deposition within the pores and result in pore-blocking since the detached particles and broken foulant particles tend to pass through the pores [33].

From the membrane damage point of view, membrane material plays a pivotal role in maintaining membrane integrity. To exemplify, PVDF is an excellent material to withstand the US irradiation despite the PES membrane, which is more susceptible to be damaged under the identical condition. Ceramic membranes are more stable than polymeric membrane under the US irradiation due to their high chemical and mechanical stability. The membrane stability under the US irradiation depends on not only the material but also the membrane structure. For instance, the membrane with larger pore size on the surface is more susceptible to US irradiation and easily damaged. The reason is the cavitation bubbles are trapped in these larger pores and after a while the surface and the spaces between pores are destroyed by bubble collapse, in turn, cracks are formed [86]. Cai et al. [7] investigated the effect of the US on the integrity of a hollow fiber membrane and compared it with a flat sheet membrane. Their finding indicated that the hollow fiber membrane was more prone to the US irradiation and some holes emerged in either inside or outside of the membrane. The hollow fibre membrane has weaker mechanical strength owing to the lack of support layer in its structure. A similar result was reported by Li et al. [159] at high US power intensity and low frequency. Another factor affecting the membrane integrity is the US operation conditions. Wang et al. [148] observed some deterioration of the US-assisted filtration performance and attributed it to the disruption of membrane integrity when the US intensity was at 1.5 W/m^2. Kyllönen et al. [130] studied the effect of the US frequency on membrane integrity in a US-assisted filtration process, in which the US transducer was placed inside the membrane module. Membrane damage at some location was observed at frequencies of 27 kHz and 40 kHz.

It was mentioned earlier that although increasing the power intensity led to higher permeate flux recovery, it may negatively affect the membrane integrity. To overcome the limitation of the ultrasound cleaning technique, the combination of a membrane surface modification method and US cleaning could be used in membrane-based processes. In fact, changing the membrane surface chemistry would help in preventing the irreversible fouling formation (by controlling the particle deposition and cake layer development). Moreover, the membrane flux could be improved by enhancing the surface hydrophilicity. As discussed in section 4.5, modifying the membrane surface will alleviate the fouling development and improve the filtration performance. Therefore, the combination of surface modification and US cleaning could be employed so as to prevent membrane damage and decrease the energy demand.

According to preceding researches, it has been proven that applying ultrasound could improve the membrane cleaning efficiency and permeate flux recovery. However, the main drawback in most of those recent studies is the method being used for the US irradiation. The practical strategy for reducing energy consumption is to use the US transducer directly on a membrane module rather than immerse the membrane module into an ultrasonic bath. In fact, the power intensity of the sound waves is attenuated as it passes through water to reach the membrane module [11]. This power reduction results in higher energy consumption and higher operating cost. Aside from the high energy requirement, using the US bath is only useful for laboratory-scale setups and it is not practical for industrial applications.

Furthermore, the detailed mechanism of particle detachment and fouling control during the US irradiation has not been fully investigated, and it needs to be addressed for prediction of the process performance, estimation of the membrane permeate flux and optimization of the filtration process. Mechanistic models are also

needed for specification of the fouling mechanism, prediction, and control of the fouling development during the filtration process.

5. Conclusion

Membrane performance improvement is not the only goal of a fouling mitigation process. Cleaning strategies that are energy efficient and have a low environmental impact are more favorable to be exploited in the future. Fouling formation and its severity depends on the type of foulants and feed solution properties, so finding an appropriate method for fouling reduction is of great importance in membrane-based separation processes. Pretreatment of the feed solution, physical cleaning, chemicals, biological agents, and surface modification are among the most commonly used fouling control strategies. In addition, ultrasound irradiation provides an alternative strategy for fouling mitigation and flux improvement. The US cleaning method does not interrupt the filtration process and is economically viable, in which no chemicals are used for foulant displacement. This method increases the membrane permeate flux by breaking the cake layer and facilitating foulant detachment from the membrane surface. However, US irradiation is not able to detach adhesive fouling on the membrane surface or within the pores. Although US irradiation is more effective at low frequency and high-power intensity, surface cracking and membrane damage may occur under these conditions. Thus, an optimal condition is required in order to obtain high cleaning efficiency, low energy consumption, and maintain membrane integrity. Furthermore, to prevent energy loss and provide practical in-situ fouling control, US transducers could be directly placed on the membrane module instead of using an US bath since the US power intensity is attenuated when passing through water. A combination of US irradiation and other cleaning methods (pre-treatment, physical and chemical cleaning, and surface modification) can be employed to improve the permeate flux without affecting the membrane integrity. Bubble dynamics and mechanism of fouling removal under the US irradiation needs to be investigated in order to either develop a mechanistic model for the US-assisted filtration processes or modify the existing models by considering all the operational parameters. The mechanistic model would help to improve the filtration efficiency by facilitating the prediction of the permeate flux and TMP changes during the filtration process.

ACKNOWLEDGEMENTS

The authors greatly appreciate the financial support from the Natural Science and Engineering Research Council of Canada (NSERC) and Department of Chemical Engineering, Ryerson University to the present project. Technical support from personnel at Ryerson University is also highly regarded.

NOMENCLATURE

Symbol Physical Meaning

A_P : cross-sectional area of a single pore [m^2]
A_m : area of membrane surface [m^2]
2a : beam width [degree]
a_0 : the initial clean membrane surface area [m^2]
B : constant related to membrane porosity and rate of removal of particles per unit area [s^{-1}]
B′ : back flux factor [s^{-1}]
C_b : bulk protein concentration [$kg \cdot m^{-3}$]
c : particle concentration [volume fraction]
c_0 : particle concentration at bulk suspension [volume fraction]
c_g : particle concentration at membrane surface [volume fraction]
c_s : sound velocity [$m \cdot s^{-1}$]
c_w : speed of the US wave [$m \cdot s^{-1}$]
D : particle diffusion coefficient [$m^2 \cdot s^{-1}$]
D_p : mean pore diameter [m]
d_{eq} : identical spherical diameter [m]
E : erosion susceptibly constant
F : fragility
f : frequency [Hz]
f′ : fraction of proteins
G : resuspension factor [s^{-1}]
H : hardness [$N \cdot m^{-2}$]
I : power intensity [$W \cdot m^{-2}$]
J : membrane permeate flux [$m \cdot s^{-1}$]
J_0 : initial permeate flux [$m \cdot s^{-1}$]
J_c, J_i, J_s : critical fluxes [$m \cdot s^{-1}$]
$J_{eq}(x)$: local equilibrium flux [$m \cdot s^{-1}$]
K_b : complete blocking constant [s^{-1}]
K_c : cake filtration constant [$s \cdot m^{-2}$]
K_i : partial blocking constant [m^{-1}]
K_s : internal blocking constant [m^{-1}]
K : constant related to the physical properties of the foulant [$m \cdot kg^{-1}(m^2 \cdot N^{-1})^{0.82}$]
k : polytropic coefficient
k_c : cake filtration constant [$kg \cdot m^{-3}$]
L : pore length [m]
m_p : mass of protein [$kg \cdot m^{-2}$]
N_{Fc} : critical filtration number
N_P : number of pores per unit area of membrane
n : available membrane pores
P : pressure [Pa]
P_C : collapse pressure [Pa]
Q : flow rate [$m^3 \cdot s^{-1}$]
$Q_{blocked}$: flow rate through the blocked area [$m^3 \cdot s^{-1}$]
Q_{open} : flow rate through the clean membrane [$m^3 \cdot s^{-1}$]
R_0 : initial cluster radius [m]
R_a : arithmetic roughness [m]
R : membrane resistance [m^{-1}]
R′ : specific protein layer resistance [$m \cdot kg^{-1}$]
R_{pp0} : resistance of a single protein aggregate [m^{-1}]
R_{pp} : resistance of protein deposit [m^{-1}]
R_{rs} : critical size of the cavitation bubble [m]
r_c : specific resistance of the cake layer [m^{-2}]
S : rate of erosion of cake per unit area [$kg \cdot m^{-2} \cdot s^{-1}$]
S_c : wall velocity of the cluster [$m \cdot s^{-1}$]
s : compressibility factor of the cake layer
T : temperature [°C]
t : time [s]
t_i : elapsed time [s]
V : permeate volume [m^3]
V_{Cav} : volume of the cavitation bubble [m^3]

v_P : flow velocity [m·s^{-1}]
W_{Cav} : energy within the cavities [J]
X_0 : volume fraction of particles in suspension

Greek Symbol

α : pore blockage parameter [m^2·kg^{-1}]
a_P : particle radius [m]
β : void fraction of the cluster
δ_m : membrane thickness [m]
δ_f : fouling layer thickness [m]
ε : membrane porosity
ε_0 : clean membrane porosity
ε_f : porosity of fouling layer
σ : area of blocked membrane per unit of the permeate volume [m^2·m^{-3}]
σ_C : shear stress created by the collapse of the cavity cluster [Pa]
σ_{EROS} : erosion stress [Pa]
μ : viscosity of water [Pa·s]
θ : fraction of energy transfer
ρ : liquid density [kg·m^{-3}]
ζ : tangential particle flux [m·s^{-1}]
γ : shear rate [s^{-1}]
φ : absorption coefficient [m^{-1}]

Subscript

c : cake layer
cp : concentration polarization
d : diamond
f : fouling layer
g : glass
ir : irreversible
m : membrane
p : membrane pores
r : reversible

REFERENCES

1. R. Zhang, Y. Huang, C. Sun, L. Xiaozhen, X. Bentian and Z. Wang, *Ultrason. Sonochem.*, **55**, 341 (2019).
2. Y. R. Chang, Y. J. Lee and D. J. Lee, *J. Taiwan Institute Chem. Eng.*, **94**, 88 (2019).
3. M. Qasim, N. N. Darwish, S. Mhiyo, N. A. Darwish and N. Hilal, *Desalination*, **443**, 143 (2018).
4. H. Li and V. Chen, *Membrane fouling and cleaning in food and bioprocessing*, Mem. Tech. Publications, Oxford (2010).
5. L. Borea, V. Naddeo, M. S. Shalaby, T. Zarra, V. Belgiorno, H. Abdalla and A. M. Shaban, *Ultrasonics*, **83**, 42 (2018).
6. X. Shi, G. Tal, N. P. Hankins and V. Gitis, *J. Water Process. Eng.*, **1**, 121 (2014).
7. M. Cai, W. Li and H. Liang, *Chem. Eng. Processing: Process Intensification*, **86**, 30 (2014).
8. N. Hengl, Y. Jin, F. Pignon, S. Baup, R. Mollard, N. Gondrexon, A. Magnin, L. Michot and E. Paineau, *Ultrason. Sonochem.*, **21**, 1018 (2014).
9. N. V. Thombre, A. P. Gadhekar, A. V. Patwardhan and P. R. Gogate, *Ultrason. Sonochem.*, **62**, 104891 (2020).
10. K. K. Latt and T. Kobayashi, *Ultrason. Sonochem.*, **13**, 321 (2006).
11. H. M. Kyllönen, P. Pirkonen and M. Nyström, *Desalination*, **181**, 319 (2005).
12. E. S. Dassoff and Y. O. Li, *Trends Food Sci. Technol.*, **86**, 492 (2019).
13. E. Alventosa-deLara, S. Barredo-Damas, M. I. Alcaina-Miranda and M. I. Iborra-Clar, *Ultrason. Sonochem.*, **21**, 1222 (2014).
14. M. J. Luján-Facundo, J. A. Mendoza-Roca, B. Cuartas-Uribe and S. Álvarez-Blanco, *Ultrason. Sonochem.*, **33**, 18 (2016).
15. D. Chen, L. K. Weavers and H. W. Walker, *Ultrason. Sonochem.*, **13**, 379 (2006).
16. H. W. D. Camara, H. Doan and A. Lohi, *Ultrasonics*, **108**, 106206 (2020).
17. K. M. Lee, H. Doan and F. Ein-Mozaffari, *Can. J. Chem. Eng.*, **98**, 1648 (2020).
18. N. Hilal, O. O. Ogunbiyi, N. J. Miles and R. Nigmatullin, *Sep. Sci. Technol.*, **40**, 1957 (2005).
19. X. Du, Y. Shi, V. Jegatheesan and I. U. Haq, *Membranes*, **10**, 24 (2020).
20. J. Brinck, A. S. Jönsson, B. Jönsson and J. Lindau, *J. Membr. Sci.*, **164**, 187 (2000).
21. R. Liang, A. Hu, M. Hatat-Fraile and N. Zhou, *Fundamentals on adsorption, membrane filtration, and advanced oxidation processes for water treatment*, Springer Publications, New York (2014).
22. Z. Wang, J. Ma, C. Y. Tang, K. Kimura, Q. Wang and X. Han, *J. Membr. Sci.*, **468**, 276 (2014).
23. R. J. Wakeman and C. J. Williams, *Sep. Purif. Technol.*, **26**, 3 (2002).
24. S. Shirazi, C. J. Lin and D. Chen, *Desalination*, **250**, 236 (2010).
25. P. Priyananda and V. Chen, *J. Membr. Sci.*, **273**, 58 (2006).
26. I. Ibrar, O. Naji, A. Sharif, A. Malekizadeh, A. Alhawari, A. A. Alanezi and A. Altaee, *Water*, **11**, 695 (2019).
27. Q. Li and M. Elimelech, *Environ. Sci. Technol.*, **38**, 4683 (2004).
28. B. Mi and M. Elimelech, *J. Membr. Sci.*, **348**, 337 (2010).
29. K. S. Katsoufidou, D. C. Sioutopoulos, S. G. Yiantsios and A. J. Karabelas, *Desalination*, **264**, 220 (2010).
30. Y. J. Choi, S. H. Kim, S. Jeong and T. M. Hwang, *Desalination*, **336**, 153 (2014).
31. L. D. Tijing, Y. C. Woo, J. S. Choi, S. Lee, S. H. Kim and H. K. Shon, *J. Membr. Sci.*, **475**, 215 (2015).
32. F. Qu, H. Liang, J. Tian, H. Yu, Z. Chen and G. Li, *Desalination*, **293**, 30 (2012).
33. A. L. Lim and R. Bai, *J. Membr. Sci.*, **216**, 279 (2003).
34. M. Bagheri and S. A. Mirbagheri, *Bioresour. Technol.*, **258**, 318 (2018).
35. P. Xu, J. E. Drewes, T. U. Kim, C. Bellona and G. Amy, *J. Membr. Sci.*, **279**, 165 (2006).
36. F. Meng, S. Zhang, Y. Oh, Z. Zhou, H. S. Shin and S. R. Chae, *Water Res.*, **114**, 151 (2017).
37. S. Lee, J. Cho and M. Elimelech, *J. Membr. Sci.*, **262**, 27 (2005).
38. A. S. Kim, A. E. Contreras, Q. Li and R. Yuan, *Langmuir*, **25**, 7815 (2009).
39. A. M. Klüpfel and F. H. Frimmel, *Desalination*, **250**, 1005 (2010).
40. E. Arkhangelsky, F. Wicaksana, C. Tang, A. A. Al-Rabiah, S. M. Al-Zahrani and R. Wang, *Water Res.*, **46**, 6329 (2012).
41. Y. Liu and B. Mi, *J. Membr. Sci.*, **407**, 136 (2012).
42. Y. Kim, M. Elimelech, H. K. Shon and S. Hong, *J. Membr. Sci.*, **460**, 206 (2014).
43. A. I. Radu, L. Bergwerff, M. C. M. Van Loosdrecht and C. Picioreanu, *Biofouling*, **31**, 83 (2015).

44. F. Zhao, K. Xu, H. Ren, L. Ding, J. Geng and Y. Zhang, *J. Membr. Sci.*, **486**, 177 (2015).
45. G. Singh and L. Song, *J. Membr. Sci.*, **303**, 112 (2007).
46. H. Lee, R. Sep and J. Kim, *Bioresour. Technol.*, **302**, 122813 (2020).
47. A. Abdelrasoul, H. Doan and A. Lohi, *Can. J. Chem. Eng.*, **92**, 1293 (2014).
48. G. Singh and L. Song, *J. Colloid Interface Sci.*, **284**, 630 (2005).
49. P. Zhao, B. Gao, Q. Yue, P. Liu and H. K. Shon, *J. Environ. Sci.*, **46**, 55 (2016).
50. J. Lee, S. Jeong, Y. Ye, V. Chen, S. Vigneswaran, T. Leiknes and Z. Liu, *Sep. Purif. Technol.*, **176**, 323 (2017).
51. C. Jönsson and A. S. Jönsson, *J. Membr. Sci.*, **108**, 79 (1995).
52. C. W. Jung, H. J. Son and L. S. Kang, *Desalination*, **197**, 154 (2006).
53. C. Hobbs, J. Taylor and S. Hong, *J. Water Supply: Res. Tech—AQUA*, **55**, 559 (2006).
54. G. Z. Ramon and E. M. V. Hoek, *J. Membr. Sci.*, **425**, 141 (2013).
55. M. Hashino, T. Katagiri, N. Kubota, Y. Ohmukai, T. Maruyama and H. Matsuyama, *J. Membr. Sci.*, **366**, 389 (2011).
56. Y. N. Wang and C. Y. Tang, *J. Membr. Sci.*, **376**, 275 (2011).
57. K. Košutić and B. Kunst, *Desalination*, **150**, 113 (2002).
58. L. D. Nghiem and S. Hawkes, *Sep. Purif. Technol.*, **57**, 176 (2007).
59. K. J. Hwang, C. Y. Liao and K. L. Tung, *Desalination*, **234**, 16 (2008).
60. K. Zeng, J. Zhou, Z. Cui, Y. Zhou, C. Shi, X. Wang, L. Zhou, X. Ding, Z. Wang and E. Drioli, *Chin. J. Chem. Eng.*, **26**, 268 (2018).
61. F. Qu, H. Liang, J. Zhou, J. Nan, S. Shao, J. Zhang and G. Li, *J. Membr. Sci.*, **449**, 58 (2014).
62. A. Ambrosi, N. S. M. Cardozo and I. C. Tessaro, *Food Bio. Tech.*, **7**, 921 (2014).
63. D. Sioutopoulos, A. Karabelas and V. Mappas, *Membranes*, **9**, 21 (2019).
64. A. Abdelrasoul, H. Doan and A. Lohi, *J. Membr. Sep. Technol.*, **2**, 134 (2013).
65. G. R. Bolton, A. W. Boesch and M. J. Lazzara, *J. Membr. Sci.*, **279**, 625 (2006).
66. Z. Chen, T. Xiao, D. Hu, J. Xu, X. Li, F. Jia, H. Wang, F. Gu, H. Su and Y. Zhang, *Water Res.*, **135**, 288 (2018).
67. L. Song and M. Elimelech, *J. Chem. Soc., Faraday Trans.*, **91**, 3389 (1995).
68. A. Jain, S. Sengupta and S. De, *Food Bio. Tech.*, **11**, 1012 (2018).
69. L. Song, *J. Membr. Sci.*, **139**, 183 (1998).
70. T. Jiang, M. D. Kennedy, W. G. J. Van der Meer, P. A. Vanrolleghem and J. C. Schippersa, *Desalination*, **157**, 335 (2003).
71. N. Hilal, H. Al-Zoubi, N. A. Darwish, A. W. Mohamma and M. Abu Arabi, *Desalination*, **170**, 281 (2004).
72. E. Iritani, *Drying Tech.*, **31**, 146 (2013).
73. I. S. Chang, R. Field and Z. Cui, *Des. Water Treat.*, **8**, 31 (2009).
74. V. B. Brião and C. R. G. Tavares, *Brazilian J. Chem. Eng.*, **29**, 393 (2012).
75. Y. J. Chang and M. M. Benjamin, *J. Environ. Eng.*, **129**, 25 (2002).
76. N. Ghaffour, *Desalination*, **167**, 281 (2004).
77. R. W. Field, D. Wu, J. A. Howell and B. B. Gupta, *J. Membr. Sci.*, **100**, 259 (1995).
78. J. Hermia, *Chem. Eng. Res. Des.*, **60**, 183 (1982).
79. C. C. Ho and A. L. Zydney, *J. Colloid Interface Sci.*, **232**, 389 (2000).
80. G. Bolton, D. LaCasse and R. Kuriyel, *J. Membr. Sci.*, **277**, 75 (2006).
81. S. Mondal and S. De, *Sep. Purif. Technol.*, **75**, 222 (2010).
82. T. A. Nguyen, S. Yoshikawa, K. Karasu and S. Ookawara, *J. Membr. Sci.*, **403**, 84 (2012).
83. K. A. Landman, C. Sirakoff and L. R. White, *Phys. Fluids A: Fluid Dynamics*, **3**, 1495 (1991).
84. A. Y. Kirschner, Y. H. Cheng, D. R. Paul, R. W. Field and B. D. Freeman, *J. Membr. Sci.*, **574**, 65 (2019).
85. M. Kallioinen and M. Mänttäri, *Sep. Sci. Technol.*, **46**, 1388 (2011).
86. K. R. Goode, K. Asteriadou, P. T. Robbins and P. J. Fryer, *Comprehensive Reviews in Food Sci. Food Safety*, **12**, 121 (2013).
87. T. Yang, C. F. Wan, J. Y. Xiong and T. S. Chung, *Sep. Purif. Technol.*, **215**, 390 (2019).
88. C. F. Wan, S. Jin and T. S. Chung, *J. Membr. Sci.*, **572**, 658 (2019).
89. M. A. Javeed, K. Chinu, H. K. Shon and S. Vigneswaran, *Desalination*, **238**, 98 (2009).
90. J. Zhang, K. Northcott, M. Duke, P. Scales and S. R. Gray, *Desalination*, **393**, 120 (2016).
91. A. Abdelrasoul, H. Doan, A. Lohi and C. H. Cheng, *Sep. Purif. Technol.*, **204**, 243 (2018).
92. R. Sondhi and R. Bhave, *J. Membr. Sci.*, **186**, 41 (2011).
93. S. Armbruster, O. Cheong, J. Lölsberg, S. Popovic, S. Yüce and M. Wessling, *J. Membr. Sci.*, **554**, 156 (2018).
94. D. M. Krstić, M. N. Tekić, M. D. Carić and S. D. Milanović, *J. Membr. Sci.*, **208**, 303 (2002).
95. A. Jokić, Z. Zavargo, Z. Šereš and M. Tekić, *J. Membr. Sci.*, **350**, 269 (2010).
96. A. Fouladitajar, F. Z. Ashtiani, H. Rezaei, A. Haghmoradi and A. Kargari, *J. Ind. Eng. Chem.*, **20**, 624 (2014).
97. Y. J. Zhao, K. F. Wu, Z. J. Wang, L. Zhao and S. S. Li, *J. Environ. Sci. (China)*, **12**, 241 (2000).
98. Z. Allie, E. P. Jacobs, A. Maartens and P. Swart, *J. Membr. Sci.*, **218**, 107 (2003).
99. M. A. Argüello, S. Alvarez, F. A. Riera and R. Alvarez, *Sep. Purif. Technol.*, **41**, 147 (2005).
100. D. Chen and M. Columbia, *J. Membr. Sci.*, **381**, 118 (2011).
101. M. Ehsani and A. Aroujalian, *Poly. Adv. Tech.*, **31**, 772 (2020).
102. X. Ding, C. Yang, T. P. Lim, L. Y. Hsu, A. C. Engler, J. L. Hedrick and Y. Y. Yang, *Biomaterials*, **33**, 6593 (2012).
103. W. Ma, S. Rajabzadeh, A. R. Shaikh, Y. Kakihana, Y. Sun and H. Matsuyama, *J. Membr. Sci.*, **514**, 429 (2016).
104. H. Sun, X. Yang, Y. Zhang, X. Cheng, Y. Xu, Y. Bai and L. Shao, *J. Membr. Sci.*, **563**, 22 (2018).
105. V. ochkodan, D. J. Johnson and N. Hilal, *Adv. Colloid Interface Sci.*, **206**, 116 (2014).
106. C. H. Yu, L. C. Fang, S. K. Lateef, C. H. Wu and C. F. Lin, *J. Hazard. Mater.*, **177**, 1153 (2010).
107. H. Ma, L. F. Hakim, C. N. Bowman and R. H. Davis, *J. Membr. Sci.*, **189**, 255 (2001).
108. A. Simon, N. Gondrexon, S. Taha, J. Cabon and G. Dorange, *Sep. Sci. Technol.*, **35**, 2619 (2000).
109. X. L. Wang, X. F. Li, X. Q. Fu, R. Chen and B. Gao, *Desalination*, **175**, 187 (2005).
110. M. O. Lamminen, H. W. Walker and L. K. Weavers, *J. Membr. Sci.*, **283**, 225 (2006).
111. Y. Gao, D. Chen, L. K. Weavers and H. W. Walker, *J. Membr. Sci.*, **401**, 232 (2012).

112. D. Feng, J. S. J. Van Deventer and C. Aldrich, *Sep. Purif. Technol.*, **50**, 318 (2006).
113. D. Hou, L. Zhang, Z. Wang, H. Fan, J. Wang and H. Huang, *Sep. Purif. Technol.*, **154**, 328 (2015).
114. V. Naddeo, L. Borea and V. Belgiorno, *J. Water. Proc. Eng.*, **8**, e92 (2015).
115. D. Hou, L. Zhang, Z. Wang, H. Fan, J. Wang and H. Huang, *Desalination*, **386**, 48 (2016).
116. D. Hou, L. Zhang, Z. Wang, H. Fan, J. Wang and H. Huang, *Sep. Purif. Technol.*, **175**, 287 (2017).
117. F. Chemat and M. K. Khan, *Ultrason. Sonochem.,* **18**, 813 (2011).
118. G. L. Chahine, A. Kapahi, J. K. Choi and C. T. Hsiao, *Ultrason. Sonochem.*, **29**, 528 (2016).
119. L. A. Teran, S. A. Rodriguez, S. Laín and S. Jung, *Phys. Fluids*, **30**, 123304 (2018).
120. B. Boyd and S. Becker, *Phys. Fluids*, **31**, 032102 (2019).
121. M. O. Lamminen, H. W. Walker and L. K. Weavers, *J. Membr. Sci.*, **237**, 213 (2004).
122. J. Collis, R. Manasseh, P. Liovic, P. Tho, A. Ooi, K. Petkovic-Duran and Y. Zhu, *Ultrasonics*, **50**, 273 (2010).
123. L. Wolloch and J. Kost, *J. Controlled Release*, **148**, 204 (2010).
124. S. B. Awad and R. Nagarajan, *Ultrasonic cleaning*, William Andrew Applied Sci. Publications, Norwich (2010).
125. P. M. Kanthale, P. R. Gogate, A. B. Pandit and A. M. Wilhelm, *Ultrason. Sonochem.*, **10**, 181 (2003).
126. P. R. Gogate and A. B. Pandit, *Ultrason. Sonochem.*, **11**, 105 (2003).
127. W. Będkowski, G. Gasiak, C. Lachowicz, A. Lichtarowicz, T. Łagoda and E. Macha, *Wear*, **230**, 201 (1999).
128. T. Kobayashi, T. Kobayashi, Y. Hosaka and N. Fujii, *Ultrasonics*, **41**, 185 (2003).
129. V. Naddeo, L. Borea and V. Belgiorno, *J. Water Process. Eng.*, **8**, e92 (2015).
130. H. Kyllönen, P. Pirkonen, M. Nyström, J. Nuortila-Jokinen and A. Grönroos, *Ultrason. Sonochem.*, **13**, 295 (2006).
131. M. Cai, S. Wang, Y. Zheng and H. Liang, *Sep. Purif. Technol.*, **68**, 351 (2009).
132. J. Heikkinen, H. Kyllönen, E. Järvelä, A. Grönroos and C. Y. Tang, *J. Membr. Sci.*, **528**, 147 (2017).
133. M. J. Luján-Facundo, J. A. Mendoza-Roca, B. Cuartas-Uribe and S. Álvarez-Blanco, *J. Sep. Purif. Technol.*, **120**, 275 (2013).
134. S. R. Gonzalez-Avila, F. Prabowo, A. Kumar and C. D. Ohl, *J. Membr. Sci.*, **415**, 776 (2012).
135. A. Maskooki, M. H. Shahraki and M. Mohamadi, *Des. Water. Treat.*, **57**, 5376 (2014).
136. Y. Matsumoto, T. Miwa, S. I. Nakao and S. Kimura, *J. Chem. Eng. Japan*, **29**, 561 (1996).
137. T. Kobayashi, T. Kobayashi and N. Fujii, *Japanese J. Appl. Phys.*, **39**, 2980 (2000).
138. R. S. Juang and K. H. Lin, *J. Membr. Sci.*, **243**, 115 (2004).
139. S. Muthukumaran, S. E. Kentish, M. Ashokkumar and G. W. Stevens, *J. Membr. Sci.*, **258**, 106 (2005).
140. A. Mirzaie and T. Mohammadi, *J. Food Eng.*, **108**, 77 (2012).
141. C. C. Kan, D. A. D. Genuino, K. K. P. Rivera and M. D. G. de Luna, *J. Membr. Sci.*, **497**, 450 (2016).
142. S. Muthukumaran, S. Kentish, S. Lalchandani, M. Ashokkumar, R. Mawson, G. W. Stevens and F. Grieser, *Ultrason. Sonochem.*, **12**, 29 (2005).
143. X. Chai, T. Kobayashi and N. Fujii, *Sep. Purif. Technol.*, **15**, 139 (1999).
144. X. Liu, Y. Hou, X. Liu, J. He, J. Lu and X. Ni, *Optik*, **122**, 1254 (2011).
145. C. Zhu and G. Liu, *J. Membr. Sci.*, **176**, 31 (2000).
146. X. M. Liu, Z. Long, J. He, B. B. Li, X. H. Liu, J. Y Zhao, J. Lu and X. W. Ni, *Optoelectronics Letters*, **9**, 317 (2013).
147. J. Li, R. D. Sanderson and E. P. Jacobs, *J. Membr. Sci.*, **205**, 247 (2002).
148. J. Wang, X. Gao, Y. Xu, Q. Wang, Y. Zhang, X. Wang and C. Gao, *Desalination*, **377**, 172 (2016).
149. A. Henglein and M. Gutierrez, *J. Phys. Chem.*, **97**, 158 (1993).
150. W. Yu, N. Graham and T. Liu, *J. Membr. Sci.*, **535**, 168 (2017).
151. S. A. Aktij, A. Taghipour, A. Rahimpour, A, Mollahosseini and A. Tiraferri, *Ultrasonics*, **108**, 106228 (2020).
152. D. Chen, L. K. Weavers and H. W. Walker, *Water Res.*, **40**, 840 (2006).
153. S. K. Mah, C. K. Chuah, W. C. Lee and S. P. Chai, *Sep. Purif. Technol.*, **98**, 419 (2012).
154. S. Lee, H. K. Shon and S. Hong, *Desalination*, **421**, 79 (2017).
155. M. H. Shahraki, A. Maskooki, A. Faezian and A. Rafe, *Des. Water. Treat.*, **57**, 24278 (2016).
156. S. Muthukumaran, K. Yang, A. Seuren, S. Kentish, M. Ashokkumar, G. W. Stevens and F. Grieser, *Sep. Purif. Technol.*, **39**, 99 (2004).
157. A. Maskooki, T. Kobayashi, S. A. Mortazavi and A. Maskooki, *Sep. Purif. Technol.*, **59**, 67 (2008).
158. M. J. Luján-Facundo, J. A. Mendoza-Roca, B. Cuartas-Uribe and S. Álvarez-Blanco, *J. Cleaner Production*, **143**, 804 (2017).
159. X. Li, J. Yu and A. A. Nnanna, *Desalination*, **281**, 23 (2011).